Research article

Estimating Fe valence in magmatic clinopyroxene crystals: Fe-XANES versus electron microprobe

David A. Neave[1]✉ Elisabetta Mariani[2] Alexander G. Stewart[1] Margaret E. Hartley[1] Oliver Shorttle[3,4] Madeleine C. S. Humphreys[5]

[1] Department of Earth and Environmental Sciences, The University of Manchester, Manchester, M13 9PL, United Kingdom
[2] Department of Earth, Ocean and Ecological Sciences, University of Liverpool, Liverpool, L69 3GP, United Kingdom
[3] Department of Earth Sciences, University of Cambridge, Cambridge, CB2 3EQ, United Kingdom
[4] Institute of Astronomy, University of Cambridge, Cambridge, CB3 0HA, United Kingdom
[5] Department of Earth Sciences, Durham University, Durham, DH1 3LE, United Kingdom

✉ **Correspondence to:** David A. Neave: david.neave@manchester.ac.uk

Author contributions: Conceptualization: DAN, MCSH; Formal analysis: DAN, EM; Funding acquisition: DAN; Investigation: DAN, EM, AGS, MEH, OS, MCSH; Resources: EM; Writing — original draft: DAN; Writing — review & editing: EM, AGS, MEH, OS, MCSH

Data, code, and outputs: Neave et al. (2026a) https://doi.org/10.48420/29852546.v4

Additional data: Neave et al. (2026b) https://doi.org/10.5285/c1900414-3e31-4d85-a2b8-3beacdf54392

Submitted: 2025-11-26
Accepted: 2026-05-26
Published: 2026-06-22

Production editor:
Ekaterina S. Kiseeva

Reviews:
Ery Hughes
and two anonymous reviewers

Copyediting:
Edith Kubik,
Marthe Klöcking

High-precision estimates of Fe valence ($Fe^{3+}/\Sigma Fe$, where $\Sigma Fe = Fe^{2+} + Fe^{3+}$) in glasses and isotropic minerals from Fe K-edge X-ray absorption near-edge structure spectroscopy (Fe-XANES) have greatly improved our understanding of magmatic fO_2 in recent years. However, isotropic phases are not always present in the rock record, and our poor understanding of $Fe^{3+}/\Sigma Fe$ in anisotropic minerals, including near-ubiquitous clinopyroxene, hampers our ability to use them to investigate magmatic fO_2. Here we evaluate strategies for using pre-edge centroid positions obtained from Fe-XANES to determine $Fe^{3+}/\Sigma Fe$ in clinopyroxene powders and oriented single crystals. First, we show that clinopyroxene $Fe^{3+}/\Sigma Fe$ can be calibrated against pre-edge centroid positions collected from powdered reference materials characterised by Mössbauer spectroscopy, albeit with a precision of 11 % (1 σ absolute). Second, spectra collected from oriented crystals reveal that centroid positions depend not only on crystal orientation but also that the nature of this dependence varies with $Fe^{3+}/\Sigma Fe$. Nevertheless, we are able to determine $Fe^{3+}/\Sigma Fe$ in unknown, but oriented, clinopyroxene crystals with precisions of 12–19 % (1 σ absolute). Applying clinopyroxene Fe-XANES to samples from Iceland and the Azores validates previously reported estimates of $Fe^{3+}/\Sigma Fe$ from stoichiometry. However, our findings confirm that determining clinopyroxene $Fe^{3+}/\Sigma Fe$ by Fe-XANES requires reference materials and unknowns to be reproducibly oriented to within a few degrees, a necessity that makes Fe-XANES ill-suited for routine analyses of clinopyroxene. We find that electron microprobe-based approaches readily and rapidly return more precise clinopyroxene $Fe^{3+}/\Sigma Fe$ determinations than the Fe-XANES approaches we describe here, and are hence more appropriate for measuring the large numbers of samples required to investigate the nature and causes of fO_2 variability in magmatic systems.

1 Introduction

The redox state of multivalent elements controls magmatic phase equilibria relations, the trajectories along which magmas evolve, the speciation of gases emitted by volcanic degassing and whether magmas form economically significant mineral deposits (e.g., Frost, 1991). The availability of oxygen in magmatic systems is generally expressed in terms of log-unit deviations in oxygen fugacity (fO_2)—a measure of the non-ideal partial pressure of O—from reference equilibria of known fO_2 such as that between fayalite, magnetite and quartz (FMQ; O'Neill, 1987). Magmas erupted in different tectonic settings often record evolution under different fO_2 conditions, with magmas from volcanic arcs recording consistently more oxidising conditions than those from mid-ocean ridges ($\sim\Delta$FMQ +1 versus $\sim$FMQ;

Wood et al., 1990; Carmichael, 1991; Cottrell et al., 2022). Oxygen fugacity systematics at ocean islands are more challenging to interpret, with some systems such as the Canary Islands being associated with relatively oxidising conditions ($\Delta FMQ > 2$) and others such as Réunion with relatively reducing conditions ($\Delta FMQ < 0$), potentially as a result of variations in mantle source composition between different settings (Brounce et al., 2017; Moussallam et al., 2019; Brounce et al., 2022; Taracsák et al., 2022). Despite considerable and accelerating progress, much about the nature and causes of fO_2 variability in magmas and their mantle sources remains uncertain.

Magmatic fO_2 conditions are generally estimated using oxybarometers that exploit redox-sensitive equilibria calibrated against experiments performed under known fO_2 conditions (e.g., Ballhaus et al., 1991; Ghiorso and Sack, 1991; Kress and Carmichael, 1991). Reactions involving Fe are of particular significance because Fe is the most abundant multivalent element in terrestrial magmas, with molar ratios of Fe^{3+} to total Fe ($Fe^{3+}/\Sigma Fe$, where $\Sigma Fe = Fe^{2+} + Fe^{3+}$) typically varying between ~ 0.1 and ~ 0.4 in magmatic liquids erupted across diverse tectonic settings (Moussallam et al., 2019; Cottrell et al., 2022). Indeed, many estimates of magmatic fO_2 have been facilitated by parameterising fO_2 as a function of the valence state of Fe in magmatic liquids (e.g., Kress and Carmichael, 1991; Borisov et al., 2018; O'Neill et al., 2018). However, using such approaches to estimate the fO_2 of primitive magmas and their mantle sources is often compromised by degassing and post-entrapment processes (crystallisation and diffusive re-equilibration) modifying the primary valence of Fe in the case of matrix glasses and melt inclusions, respectively (Moussallam et al., 2016; Hartley et al., 2017; Helz et al., 2017). More fundamentally, oxybarometers predicated on the properties of magmatic liquids can only be applied to samples containing pristine glasses, considerably limiting their utility. While magmatic fO_2 can also be estimated from olivine V contents, spinel compositions and magnetite-ilmenite pairs (e.g., Ghiorso and Evans, 2008; Nikolaev et al., 2016; Nicklas et al., 2022), these approaches still require specific mineral phases to be present.

Clinopyroxene—$M2(R^{2+})M1(R^{2+})T_2(2R^{4+})O_6$, where R is a metal cation, M2 is a distorted octahedral site, M1 is a regular octahedral site and T is a tetrahedral site typically occupied by Si—crystallises from myriad magmas, and can accommodate both Fe^{2+} and Fe^{3+} onto its M1 site through diverse substitutions (Morimoto et al., 1988); Fe is not generally accommodated within the considerably larger M2 site. Reactions involving clinopyroxene thus represent appealing candidates for developing new oxybarometers that can be applied to a wide range of magmatic systems, including those lacking pristine glasses. Recent high-precision stoichiometric estimates of clinopyroxene $Fe^{3+}/\Sigma Fe$ contents from oceanic samples demonstrate that $Fe^{3+}/\Sigma Fe$ in magmatic crystals spans a range of at least 0.0–0.5 (Neave et al., 2024b), with crystals from more oxidising settings (Pico Island in the Azores) generally recording higher $Fe^{3+}/\Sigma Fe$ contents than crystals from relatively reducing settings (Icelandic rift zones). However, developing clinopyroxene-based oxybarometers is complicated by the steric effects imposed by the clinopyroxene crystal structure, as noted by early attempts to calibrate a clinopyroxene-based oxybarometer for Martian magmas (McCanta et al., 2004). In order to systematically examine such steric effects, we need to be able to determine the $Fe^{3+}/\Sigma Fe$ content of clinopyroxene crystals rapidly and routinely as well as accurately and precisely.

The increasingly routine application of synchrotron-based high-sensitivity X-ray absorption near-edge structure spectroscopy on the Fe K-edge (Fe-XANES) has improved our ability to determine $Fe^{3+}/\Sigma Fe$ in large numbers of geological samples over the past 20 years (e.g., Wilke et al., 2007; Cottrell et al., 2009; Sutton et al., 2020). Crucially, the small size of Fe-XANES spots (beam diameters and penetration depths in fluorescence are often no more than 10 μm and 50 μm, respectively) has facilitated the analysis of matrix glasses and melt inclusions in a wide range of petrogenetic contexts, greatly enriching our understanding of fO_2 in magmatic systems (Kelley and Cottrell, 2009; Cottrell and Kelley, 2011; Moussallam et al., 2014; Shorttle et al., 2015; Hartley et al., 2017). Although information about Fe valence is encoded across the Fe K-edge, most published studies have focussed on calibrating the centroid position of pre-edge structures located $\sim$15–20 eV before the main K-edge (e.g., Westre et al., 1997; Wilke et al., 2001). The form of these pre-edge structures reflects how the energy of the $1s \rightarrow 3d$ pre-edge transition changes with Fe valence, such that centroid positions are typically 1.4 eV higher for Fe^{3+} compounds than Fe^{2+} compounds (Wilke et al., 2001). Although the structure of the pre-edge region is also affected by $1s \rightarrow 4d$ transitions (Westre et al., 1997; Berry et al., 2003), simple calibrations of centroid position as functions of $Fe^{3+}/\Sigma Fe$ constructed with matrix-matched reference materials can generally recover the $Fe^{3+}/\Sigma Fe$ of unknown glasses with precisions of 1 % (1 σ absolute) or better (Cottrell et al., 2009; Zhang et al., 2018); equivalent results have also been obtained through principle component regression of the entire pre-edge region (Shorttle et al., 2015).

The high spatial resolution of Fe-XANES makes it possible to analyse individual mineral grains (Dyar et al., 2002), and analyses performed on isotropic spinel and garnet have proven particularly fruitful for investigating Fe valence and fO_2 in mantle rocks (Berry et al., 2010; Sorbadere et al., 2018; Holycross and Cottrell, 2022). Moreover, analysing nominally anhydrous minerals such as spinel circumvents beam-induced redox changes described from analyses of hydrous glasses (Shorttle et al., 2015; Cottrell et al., 2018; Blundy et al., 2020). However, performing Fe-XANES analyses on minerals is often more challenging than performing technically equivalent analyses on glasses. For example, the intensity of pre-edge structures depends strongly on Fe coordination as well as on Fe valence through their sensitivity to bonding environments: tetrahedral Fe (^{IV}Fe) features are considerably more intense than octahedral Fe (^{VI}Fe) features at equivalent Fe valence because of changes in

site geometry (Wilke et al., 2001), while Fe^{3+} features are considerably more intense than Fe^{2+} features at equivalent Fe coordination because of changes in centro-symmetry (Berry et al., 2003). Therefore, centroid positions depend not only on Fe valence but also on Fe coordination, meaning that Fe must have the same coordination in unknowns and reference materials. The polarisation of X-ray beams used to perform Fe-XANES also means that spectra collected from anisotropic minerals such as pyroxene, amphibole and mica are highly orientation-dependent unless they are ground to fine powders and analysed as quasi-isotropic materials (Wilke et al., 2001; Dyar et al., 2002). For example, uncertainties in $Fe^{3+}/\Sigma Fe$ from unoriented clinopyroxene crystals may be as high as 20 % (1 σ absolute; McCanta et al., 2004), considerably greater than the ~7 % (1 σ absolute) and ~6 % (1 σ absolute) uncertainties associated with determinations from stoichiometry and Lβ/Lα flank ratios (the so-called flank method), respectively, that can be readily obtained by electron probe microanalysis (EPMA; Lamb et al., 2024; Neave et al., 2024a; Cao et al., 2025). Recent studies have allowed the effects of orientation and Fe valence to be separated by explicitly incorporating orientation data precise to a few degrees into $Fe^{3+}/\Sigma Fe$ calibrations as well as considering the structure of higher-energy XAS regions (Dyar et al., 2016; Steven et al., 2022; Ito et al., 2025). However, the difficulty of precisely orienting large numbers of unknowns and reference materials makes performing high-throughput Fe-XANES on redox-sensitive but anisotropic minerals like clinopyroxene challenging at best and impractical at worst.

Here we explore strategies for using Fe-XANES to estimate the $Fe^{3+}/\Sigma Fe$ content of powdered clinopyroxene crystals and clinopyroxene crystals with their a-c planes oriented as close to parallel with the beamline optics as possible without access to specialist equipment. The key question we seek to address is if routinely implementable Fe-XANES offers any advantages in terms of precision over recently re-validated approaches for estimating $Fe^{3+}/\Sigma Fe$ in magmatic clinopyroxene crystals by EPMA, whether by stoichiometry or the flank method. Our motivation for pursuing this question is rooted in pragmatism. The ultimate goal of our work is not to understand the X-ray optical properties of clinopyroxene (cf., Steven et al., 2022), but rather to understand redox-sensitive phase equilibria involving clinopyroxene, which depends on being able to estimate clinopyroxene $Fe^{3+}/\Sigma Fe$ contents in large numbers of samples routinely and precisely. Overall, we find that performing Fe-XANES on clinopyroxene powders and oriented single crystals can return reasonable $Fe^{3+}/\Sigma Fe$ estimates. However, without access to a large number of well-characterised reference materials and the ability to precisely orient clinopyroxene crystals to within a few degrees, synchrotron-based Fe-XANES is considerably less precise than EPMA-based approaches for determining clinopyroxene $Fe^{3+}/\Sigma Fe$ contents.

2 Samples

Endmember and single-crystal clinopyroxene samples were sourced from mineral collections at the Manchester Museum and the Department of Earth and Environmental Sciences at the University of Manchester. These samples were described in detail by Neave et al. (2024a) who reported major element compositions from EPMA and Fe valence determinations from stoichiometry (Droop, 1987) and Mössbauer spectroscopy. Specifically, this sample suite consists of one diopside single crystal (Diopside), two aegirine single crystals (Aegirine 1 and 2) and two augite single crystals (Augite 1 and 2) alongside one block of intergrown hedenbergite crystals (Hedenbergite) and one block of intergrown clinopyroxene crystals of unknown affinity (Other; Tables 1 and 2). Single crystals were cut into at least four pieces, with three pieces being visually and orthogonally oriented according to their crystal faces and mounted in epoxy, and a fourth piece being powdered under isopropanol and then sandwiched between cellophane stretched over ~0.5 mm-diameter holes drilled in Pb foil. An additional augite crystal (Augite 3) was prepared in a similar way, with visually oriented crystals being mounted in epoxy, though no powdered sample was prepared for this crystal (Table 2).

In order to evaluate the relative effects of Fe valence and coordination on Fe K-edge pre-edge structures observed by Fe-XANES (e.g., Wilke et al., 2001), a further three single-crystal samples—Olivine, Staurolite and Sanidine—were powdered and mounted between cellophane in drilled Pb foil as described above (Table 3); larger fragments were retained and mounted in epoxy for characterisation by EPMA. Olivine and staurolite samples were sourced from the Manchester Museum and the Department of Earth and Environmental Sciences at the University of Manchester, respectively. The olivine sample was collected from a mantle xenolith erupted in Auvergne, France, and contains $^{VI}Fe^{2+}$, whereas the staurolite was collected from Mt Campione in Ticino, Italy, and contains $^{IV}Fe^{2+}$. A gem-quality sanidine purchased from GGGems contains $^{IV}Fe^{3+}$, and the aegirine samples already characterised by Neave et al. (2024a) and presented in Table 1 contain $^{VI}Fe^{3+}$.

Magmatic clinopyroxene crystals were measured in two polished thin sections previously described by Neave et al. (2024b): Skuggaföll in Iceland and Pico Island in the Azores. The sample from Skuggafjöll (SKU) is a tholeiitic and moderately primitive pillow basalt collected from the Eastern Volcanic Zone of Iceland (Neave et al., 2014). The sample from Pico (PI-011) is an alkali basalt collected from the northern flank of the Pico volcano (van Gerve et al., 2024). Stoichiometry suggests that these samples are associated with $Fe^{3+}/\Sigma Fe$ contents of ~0.00–0.30 and ~0.15–0.45, respectively, in line with alkalic systems generally having higher Fe^{3+} contents than tholeiitic systems.

Table 1. Mean major element compositions of Aegirine 1, Aegirine 2, Augite 1 and Augite 2 determined by EPMA ($\bar{x}$) and reported by Neave et al. (2024a); Fe_2O_3 and FeO contents were determined by EPMA following Droop (1987). Uncertainties in major element compositions were determined by repeat analysis and are expressed at the 1 σ level; these uncertainties are equal to or greater than those propagated from analyses of individual spots. Molar ferric-to-total iron ($Fe^{3+}/\Sigma Fe$) contents from EPMA and Mössbauer spectroscopy are reported as molar proportions. Uncertainties in $Fe^{3+}/\Sigma Fe$ contents determined by Mössbauer spectroscopy were derived from MossA fitting (Prescher et al., 2012).

Oxides	Aegirine 1		Aegirine 2		Augite 1		Augite 2	
EPMA	$\bar{x}$	1σ	$\bar{x}$	1σ	$\bar{x}$	1σ	$\bar{x}$	1σ
SiO_2 (wt. %)	52.07	0.33	52.06	0.26	46.73	0.58	47.61	0.69
TiO_2	2.33	0.26	3.11	0.09	2.15	0.18	2.81	0.26
Al_2O_3	0.21	0.03	0.16	0.02	8.04	0.58	5.97	0.58
Cr_2O_3	0.00	0.01	0.00	0.01	0.17	0.18	0.04	0.03
Fe_2O_3	25.34	0.34	25.86	0.32	3.84	0.35	3.13	0.34
FeO	4.52	0.25	2.85	0.24	3.21	0.31	3.95	0.30
MnO	1.09	0.10	1.70	0.06	0.11	0.02	0.11	0.01
MgO	0.21	0.07	0.06	0.01	12.75	0.50	13.45	0.29
CaO	1.49	0.38	0.28	0.03	22.86	0.22	22.75	0.15
Na_2O	12.17	0.24	12.94	0.08	0.54	0.08	0.49	0.04
Total	99.43		99.03		100.39		100.32	
$Fe^{3+}/\Sigma Fe$ Mössbauer	0.84	0.03	0.93	0.03	0.56	0.03	0.42	0.03
$Fe^{3+}/\Sigma Fe$ EPMA	0.83	0.01	0.89	0.01	0.52	0.05	0.42	0.04

Table 2. Mean major element compositions of Diopside, Hedenbergite and the Other clinopyroxene determined by EPMA ($\bar{x}$) and reported by Neave et al. (2024a); Fe_2O_3 and FeO contents were determined by EPMA following Droop (1987). Equivalent compositions are also reported for Augite 3. Molar ferric-to-total iron ($Fe^{3+}/\Sigma Fe$) contents from EPMA and Mössbauer spectroscopy are reported as molar proportions. Uncertainties in these samples were determined in the ways described in the caption of Table 1. *The Fe_2O_3 content of Diopside is below the detection limit of EPMA.

Oxides	Diopside		Hedenbergite		Other		Augite 3	
EPMA	$\bar{x}$	1σ	$\bar{x}$	1σ	$\bar{x}$	1σ	$\bar{x}$	1σ
SiO_2 (wt. %)	54.90	0.19	48.96	0.23	55.43	0.39	49.15	0.78
TiO_2	0.01	0.03	0.00	0.03	0.00	0.02	1.15	0.17
Al_2O_3	0.56	0.13	0.65	0.11	0.31	0.10	4.80	0.61
Cr_2O_3	0.41	0.28	0.00	0.01	0.00	0.01	0.02	0.02
Fe_2O_3	0.00*	0.00	0.81	0.32	0.70	0.33	3.27	0.33
FeO	3.38	0.16	25.57	0.27	0.59	0.28	5.79	0.29
MnO	0.11	0.02	0.89	0.04	0.59	0.30	0.19	0.02
MgO	16.13	0.16	1.24	0.09	17.86	0.50	13.36	0.42
CaO	25.05	0.25	22.41	0.29	25.73	0.34	22.16	0.20
Na_2O	0.27	0.09	0.25	0.06	0.07	0.04	0.35	0.01
Total	100.82		100.79		101.27		100.25	
$Fe^{3+}/\Sigma Fe$ Mössbauer	0.03	0.02	0.05	0.02	0.50	0.05		
$Fe^{3+}/\Sigma Fe$ EPMA	0.00	0.05	0.03	0.01	0.49	0.25	0.34	0.03

Table 3. Mean major element compositions of Olivine, Staurolite and Sanidine determined by EPMA ($\bar{x}$) with total Fe reported as FeO_T, where all Fe is reported as FeO. Uncertainties in major element compositions were determined by repeat analyses and are expressed at the 1 σ level for all elements. Molar ferric-to-total iron ($Fe^{3+}/\Sigma Fe$) contents from Mössbauer spectroscopy are reported as molar proportions. Uncertainties in $Fe^{3+}/\Sigma Fe$ contents determined by Mössbauer spectroscopy were derived from MossA fitting (Prescher et al., 2012).

Oxides	Olivine		Staurolite		Sanidine	
EPMA	$\bar{x}$	1σ	$\bar{x}$	1σ	$\bar{x}$	1σ
SiO_2 (wt. %)	41.10	0.14	27.79	0.28	65.35	0.25
TiO_2	0.02	0.02	0.66	0.08	0.05	0.01
Al_2O_3	0.02	0.01	54.46	0.40	17.47	0.16
Cr_2O_3	0.02	0.01	0.01	0.01		
FeO_T	9.22	0.11	13.05	0.19	1.19	0.03
MnO	0.13	0.01	0.13	0.03		
MgO	49.83	0.13	2.24	0.13	0.02	0.01
CaO	0.06	0.01				
Na_2O					0.59	0.03
K_2O					16.21	0.08
NiO	0.39	0.01				
Total	100.80		98.35		100.83	
$Fe^{3+}/\Sigma Fe$ Mössbauer	0.03	0.02	0.01	0.01	1.00	0.05

3 Methods

3.1 Scanning electron microscopy and electron probe microanalysis

Backscattered electron (BSE) images were collected from epoxy mounts and thin sections using an FEI Quanta 650F scanning electron microscope (SEM) in the Department of Earth and Environmental Sciences at the University of Manchester. Clinopyroxene, olivine, staurolite and sanidine compositions were determined by EPMA using a JEOL JXA8530F instrument in the School of Earth Sciences at the University of Bristol operated with Probe for EPMA (https://www.probesoftware.com/). Analyses were performed following the procedure described by Neave et al. (2024a), and some analyses discussed here have already been reported by Neave et al. (2024a) and Neave et al. (2024b). Clinopyroxene, staurolite and olivine crystals were analysed using an accelerating voltage of 15 kV, a beam size of 1 μm and a current of 10 nA for major elements (Si, Al, Fe, Ng, Ca) and K, and a current of 40 nA for minor elements (Cr, Mn, Na, P and Ni). On-peak counting times in seconds were as follows and twice off-peak counting times: Si (20), Ti (20), Al (20), Cr (60), Fe (40), Mn (30), Mg (40), Ca (20), Na (60), K (40), P (60) and Ni (30). Total acquisition time per clinopyroxene analysis was on the order of 7 minutes. The sanidine crystal was analysed using an accelerating voltage of 15 kV, a beam size of 10 μm and a current of 10 nA for all elements. On-peak counting times in seconds were as follows and twice off-peak counting times: Si (10), Ti (50), Al (10), Cr (10), Fe (30), Mn (30), Mg (50), Ca (10), Na (10), K (10) and P (40). Accuracy was monitored using in-house diopside, Cr-diopside and labradorite reference materials and the international KK1 kaersutite reference material (Reay et al., 1989). Major elements were generally within 2 % of preferred values obtained through years of repeat analyses or reported in the literature (Reay et al., 1989), and minor elements were within 6 %. Counting statistics from analyses of unknown crystals indicate that major and minor elements were determined with precisions better than 1 % and 5 % (1 σ relative), respectively, in individual spots (except for MnO, which was determined with a 1 σ precision of 8 %). Analyses of unknowns and reference materials are provided in Neave et al. (2026a).

3.2 Mössbauer spectroscopy

Clinopyroxene $Fe^{3+}/\Sigma Fe$ contents determined by Mössbauer spectroscopy for the materials used in this study have already been reported by Neave et al. (2024a). Additional determinations for Olivine, Staurolite and Sanidine are reported here to define the effects of Fe valence and coordination on pre-edge structures of the Fe K-edge (e.g., McCammon, 2021). In short, spectra were collected using a constant acceleration Mössbauer spectrometer with a nominal 450 MBq ^{57}Co high specific activity source in a 12 μm-thick Rh matrix in the Bayerisches Geoinstitut at the Universität Bayreuth. Velocities were calibrated against a 25 μm-thick α-Fe foil and outer line widths for the α-Fe foil were determined at room temperature. Spectra were fitted with the MossA programme (Prescher et al., 2012). Fits using variable numbers of pseudo-Voigt doublets were optimised to determine relative areas for total Fe^{2+} and Fe^{3+}. The olivine spectrum can be fitted using a doublet assigned to Fe^{2+} and a singlet assigned to Fe^{3+} that is likely associated with an Fe^{3+}-bearing impurity. The staurolite spectrum can be fitted with two doublets, both assigned to Fe^{2+}, though an additional doublet assigned to Fe^{3+} can be added without affecting the quality of the fit. The sanidine

spectrum shows evidence for magnetic ordering, and was thus collected over a wider velocity range. It can be fitted using one sextet, one broad singlet and one doublet that are all assigned to Fe^{3+}. The quality of fits to Mössbauer spectra indicates that analytical uncertainties in $Fe^{3+}/\Sigma Fe$ determinations were between 2 % and 5 % (1 σ absolute) for all powdered sample, including those reported by Neave et al. (2024a). Details of Mössbauer fits are provided in Neave et al. (2026a).

3.3 Electron backscatter diffraction

Epoxy mounts containing oriented single-crystal pieces, and thin sections from Skuggafjöll and Pico, were characterised by electron backscatter diffraction (EBSD; Prior et al., 1999, 2009). Analyses were carried out using a Zeiss GeminiSEM 450 instrument equipped with an Oxford Instruments Symmetry 2 EBSD detector in the Scanning Electron Microscopy Shared Research Facility (SEM SRF) at the University of Liverpool. Prior to performing EBSD, all samples were polished with colloidal silica, then coated with a thin layer of carbon. Samples were analysed at an angle of 70° to horizontal, using an accelerating voltage of 20 kV, a beam current of 10 nA, and working distance between 14 mm and 20 mm. The orientations of single-crystal specimens were determined by collecting maps approximately 100 × 100 μm in size with a 0.5 μm step size, to confirm the uniformity of crystallographic orientations in the crystal interiors. The orientations of crystals in thin sections and intergrown crystals in epoxy blocks were determined by mapping large areas (up to 2 cm × 3 cm) with a step size of 25 μm for the thin sections and 15 μm for the epoxy blocks. Only clinopyroxene was indexed in the single-crystal maps, using diopside, augite or aegirine datasets as required, whereas augite, labradorite, forsteritic olivine, ilmenite and magnetite were indexed in the large area thin section maps. Indexing was performed with Oxford Instruments AZtec software, and EBSD data analysis with Oxford Instruments AZtec Crystal software. All datasets were cleaned and rotated 180° around the z direction to align the EBSD reference frame with the SEM reference frame. Absolute crystallographic orientations of clinopyroxene single crystals and grains within thin sections were displayed using equal-angle upper hemisphere pole figures, phase maps, Euler angle maps and inverse pole figure maps. Summaries of EBSD results are provided alongside raw data in Neave et al. (2026a).

3.4 X-ray absorption near-edge structure

Synchrotron X-rays were used to characterise pre-edge structures of the Fe K-edge in powdered crystals, single-crystal pieces and crystals within thin sections on Beamline I18 at Diamond Light Source (DLS) during a single four-day session in February 2023. Single-crystal pieces and crystals within thin sections were analysed using a nominal ~5 × 3 μm beam while powdered crystals were analysed with a defocussed ~50 × 50 μm beam to more closely mimic analysing isotropic materials. X-ray intensity was measured over an energy range of 7020–7400 eV, using an energy step of 0.5 eV and a counting time of 2 s per

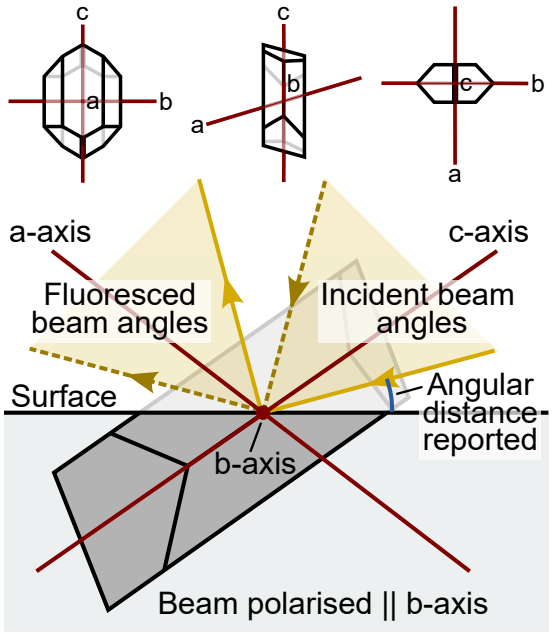

Figure 1. Sketch showing the ideal geometry used during Fe-XANES analyses of oriented clinopyroxene crystals alongside illustrative sketches showing relationships between clinopyroxene crystal faces and crystallographic axes. Crystals were mounted with a- and c-axes oriented upwards from sample surfaces and b-axes oriented parallel to the sample surface. Fe-XANES spectra were collected at a range of angles around and between the a- and c-axes that were controlled by the geometry of the beamline optics. Spectra were collected with incident beams in arcs of 60° centred at 45° from the sample surface by tilting the sample surface and rotating the sample by 180° in the plane of the sample surface. Fluoresced beams were measured at 90° to the incident beams.

step over the 7105–7120 eV energy range that is critical for defining pre-edge structures. Each clinopyroxene analysis took approximately 25 minutes, with additional time required to orient single crystal samples. The incident X-ray beam was monochromatised using a Si(311) crystal to increase the energy resolution. Aluminium plates were used to attenuate the beam to avoid saturating the detector, with a 0.1 mm-thick plate used for relatively Fe-poor samples like Augite 1 and Diopside, and a 0.25 mm-thick plate used for relatively Fe-rich samples like Aegirine 2 and Hedenbergite. Fluoresced X-rays were analysed with a Vortex ME-4 silicon drift detector positioned at 90° to the incident beam giving an ideal 90° incident-to-fluoresced X-ray geometry. These analytical conditions translated into a photon flux of 10^9–10^{10} ph/s.

Cellophane-wrapped sheets of Pb foil containing powdered samples were placed at a 45° angle to incident X-rays. Single-crystal pieces were placed at a 45° angle to incident X-rays such that the a-c planes of clinopyroxene crystals were as closely aligned to the plane defined by the beamline optics as possible (i.e., a-c planes were in the plane defined by the incident and fluoresced beams); the incident beam

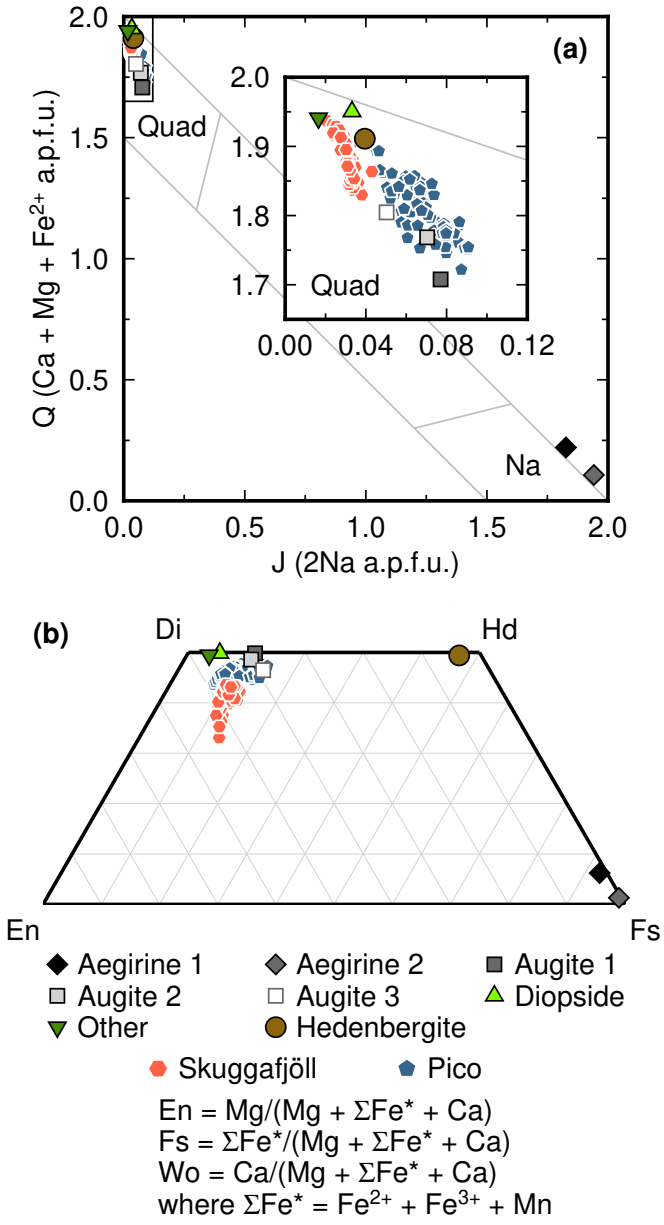

Figure 2. Major element compositions of clinopyroxene crystals. Single-crystal compositions are plotted as means of analyses reported by Neave et al. (2024a), except for Augite 3 whose compositions are reported in Table 2. Compositions of crystals in thin sections from Sküggafjöll and Pico are reported as individual spot analyses. (a) Q-J diagram used to distinguish alkali clinopyroxenes in the Na region from quadrilateral clinopyroxenes in the Quad region (Morimoto et al., 1988); all studied clinopyroxene crystals are dominated by quadrilateral components apart from Aegirine 1 and Aegirine 2. (b) Pyroxene quadrilateral showing the relative proportions of diopside (Di), hedenbergite (Hd), enstatite (En) and ferrosilite (Fs) components in studied crystals; most compositions lie close to the Di–Hd tieline apart from two aegirine single crystals.

was polarised orthogonally to the beamline optics (Figure 1). We had originally planned to use a universal stage to optimise sample orientations at the beamline, but this stage was unexpectedly unavailable. Orientation was therefore carried out visually, with clinopyroxene a-c planes and beamline optics visually oriented with a precision conservatively estimated as better than ±15°. This precision is considerably worse than that described in recent studies on oriented clinopyroxene crystals (Ito et al., 2025; Steven et al., 2022). However, we stress that the main goal of this study was to evaluate the feasibility of using Fe-XANES to generate high-throughput estimates of clinopyroxene $Fe^{3+}/\Sigma Fe$ contents using routinely available equipment rather than precisely constrain the X-ray optics of clinopyroxene (cf. Steven et al., 2022). We nevertheless investigated the effects of anisotropy within the a-c plane by rotating samples in the plane of the beamline optics with a unidirectional stage. We were therefore able to collect spectra in 60° arcs centred on samples being oriented at 45° to the incident beam. Although tilting the samples in this way stretched the nominal $\sim 5 \times 3\,\mu$m beam across the sample surface, the analysed samples were large and optically homogenous over several 10 s μm, meaning that analyses were not compromised by, for instance, mixed analyses with included phases. Rotating samples beyond 30° drastically reduced the detection of fluoresced X-rays. Further angles within the a-c plane of single crystals were accessed by remounting each crystal at an angle of 180° to their initial orientation. Crystals within thin sections were oriented by aligning the a-c planes of crystals with the beamline optics, though without access to a universal stage, we could achieve this only imperfectly and for a handful of crystals.

X-ray spectra were processed with Larch XAS viewer (Newville, 2013). First, an energy correction of 0.8 eV was applied to all spectra by fixing the E0 position (i.e., the maximum in the first derivative of the spectrum) of Fe foil at 7112.0 eV. Spectra were normalised by fitting a linear model to the region 150–280 eV above the E0 position of each spectrum. Pre-edge structures were then fitted by defining regions over which to fit a background curve with linear and Lorentzian components (typically 7106–7107 and 7117–7119 eV), and then fitting two or three Lorentzian components to pre-edge structures depending on their complexity; the structure of residuals was used to determine if extra components were needed to obtain adequate fits. Adding additional Lorentzian components did not improve the quality of our fits, even when expected from theory. Although we experimented with using batch approaches to process multiple spectra, we found that pre-edge structures and main K-edge positions and shapes varied so much between samples of different composition and orientation that processing each spectrum individually generated the most robust results. For example, the Fe^{2+}-rich Hedenbergite sample was fitted best with three components at centred low energies (7110–7112 eV) and a K-edge background pinned at relatively low energies (~7106 and ~7117), while Fe^{3+}-rich Sanidine sample was fitted best with two components centred at higher energies (7112–7114 eV) and a K-edge background pinned at relatively higher energies (~7107 and ~7119), in line with prior observations (Wilke et al., 2001). Centroid positions and fitting parameters are provided in Neave et al. (2026a).

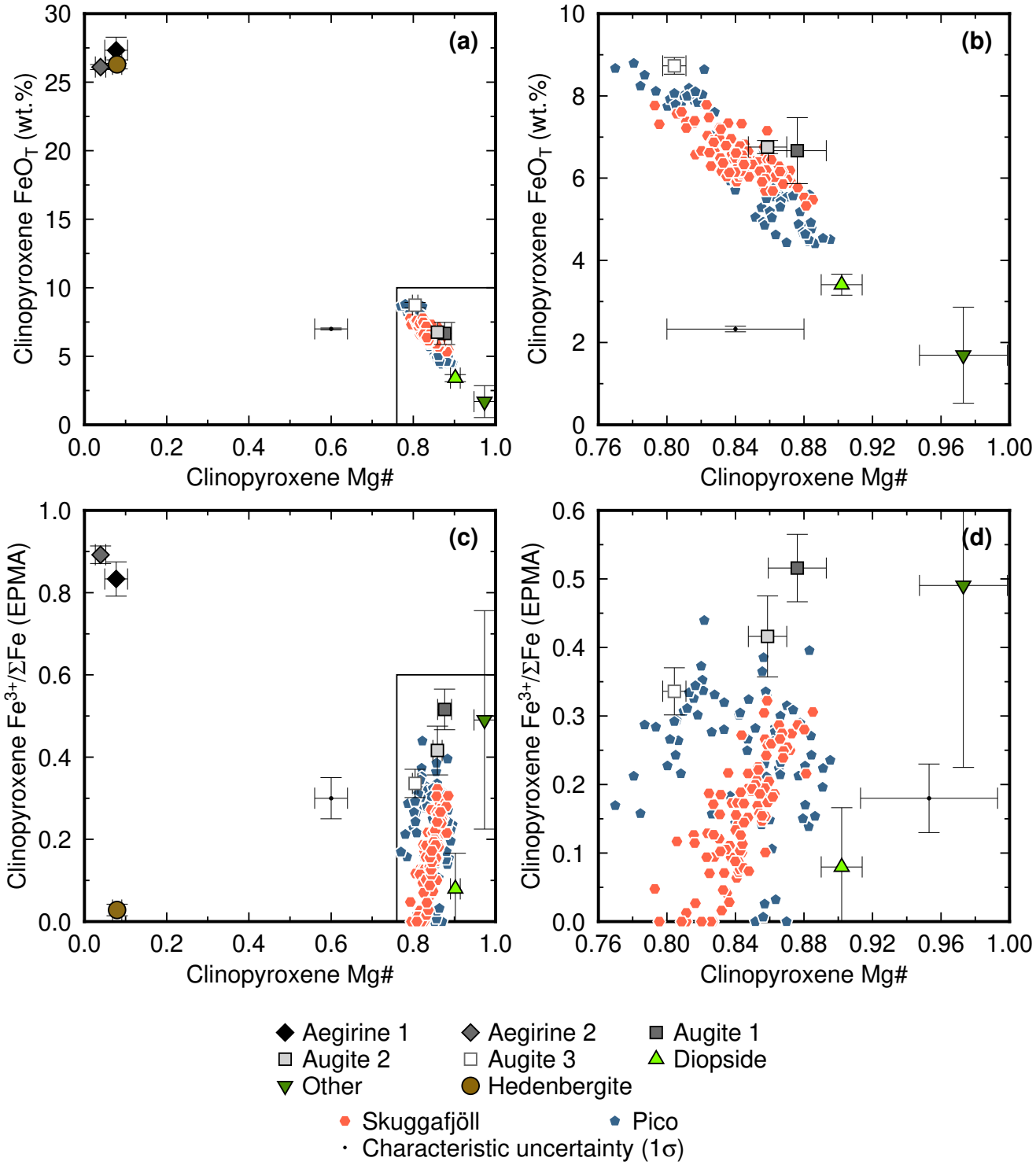

Figure 3. Concentration and valence state systematics of Fe in clinopyroxene crystals. Endmember and single-crystal compositions are plotted as means of analyses reported by Neave et al. (2024a) except for Augite 3 whose compositions are reported in Table 2; error bars are 1 σ uncertainties estimated from repeat analyses and are shown on a per-sample basis. Uncertainties in $Fe^{3+}/\Sigma Fe$ from repeat analyses of endmember and single-crystal samples are equal to or greater than those propagated from analyses of individual spots. Compositions of crystals in thin sections from Sküggafjöll and Pico are reported as individual spot analyses; characteristic 1 σ uncertainties propagated from analyses of individual spots in thin sections are shown as error bars from a small black symbol. (a and b) Systematics in clinopyroxene total Fe (FeO_T) contents as a function of Mg# (where Mg# = $Mg/(Mg+Fe^{2+})$ on a molar basis). Panel (b) shows the marked region of panel (a) in greater detail. (c and d) Systematics in clinopyroxene Fe valence as a function of Mg#. Panel (c) shows the marked region of panel (d) in greater detail.

4 Results and discussion

Major element compositions of clinopyroxene crystals are summarised in Figure 2. With the exception of our two aegirine samples, all clinopyroxene single-crystal samples analysed are dominated by the quadrilateral components diopside, hedenbergite, enstatite and ferrosilite (Figure 2a; Morimoto et al., 1988). Clinopyroxene compositions reported for our thin sections from Skuggafjöll and Pico are also dominated by quadrilateral components (Figure 2a; Neave et al., 2024b). Most of our single-crystal samples plot on a tieline between diopside and hedenbergite on a pyroxene quadrilateral, with our augite single crystals being richer in Mg than Fe (Figure 2b). Crystals in thin sections from Skuggafjöll and Pico plot close to augite single crystals on a pyroxene quadrilateral but, especially in the case of Skuggafjöll, contain higher quantities of enstatite and ferrosilite components.

The concentration and valence state systematics of Fe in clinopyroxene crystals are summarised in Figure 3. Hedenbergite and our aegirine samples are rich in total Fe (FeO_T > 25 wt.%) while Diopside is, unsurprisingly, very poor in FeO_T (<2 wt.%). Our augite samples lie between these extremes (4–9 wt.%; Figures 3a and 3b), and bracket the range of FeO_T contents in clinopyroxene crystals from Skuggafjöll and Pico. According to stoichiometric determinations obtained via EPMA, almost all of the Fe in the Hedenbergite and Diopside is Fe^{2+}, while almost all of the Fe in the aegirine samples is Fe^{3+} (Figures 3c and 3d), findings entirely validated by Mössbauer spectroscopy (Table 2). According to EPMA, Augite 1 and Augite 2 have $Fe^{3+}/\Sigma Fe$ contents of ∼0.52 and ∼0.42, respectively. Within uncertainty, these values are wholly consistent with those from Mössbauer spectroscopy (∼0.56 and ∼0.42, respectively; Table 1). Individual analyses of augitic clinopyroxene crystals from Skuggafjöll and Pico span a wider range of $Fe^{3+}/\Sigma Fe$ contents from 0.00 to 0.45, with values from Pico being slightly higher on average than those from Skuggafjöll (Neave et al., 2024b).

4.1 Powdered samples of known Fe valence

Normalised Fe-XANES spectra of powdered crystals collected across the pre-edge region of the Fe K-edge are presented in Figure 4. Spectra without background corrections demonstrate how the position of the K-edge shifts towards higher energies as Fe valence increases from Fe^{2+} in Staurolite, Olivine and Hedenbergite to Fe^{3+} in Sanidine and our aegirine samples, necessitating sample-specific background fitting (Figures 4a and 4b). Background-corrected spectra further highlight differences in the intensity of pre-edge structures between samples containing Fe with different valence and coordination states (Figures 4c and 4e). For example, the intensity of pre-edge structures at any given valence is greater in samples containing tetrahedrally coordinated Fe rather than octahedrally coordinated Fe, such that Staurolite ($^{IV}Fe^{2+}$) presents more intense pre-edge structures than Olivine ($^{VI}Fe^{2+}$). Moreover, pre-edge features are more intense in samples containing Fe^{3+} than samples containing Fe^{2+} such that aegirine samples ($^{VI}Fe^{3+}$) present more intense pre-edge structures than Olivine ($^{VI}Fe^{2+}$). Augite samples contain a mixture of Fe^{2+} and Fe^{3+} in octahedral coordination and thus present pre-edge structures of intermediate intensity (Figures 4d and 4f). Such differences in intensity are well documented in geological materials and result from changes in site geometry and centro-symmetry (Westre et al., 1997; Wilke et al., 2001; Berry et al., 2003).

Examples of fits to pre-edge structures in spectra collected from powdered clinopyroxene samples with $Fe^{3+}/\Sigma Fe$ contents ranging from ∼0.05 to ∼0.93 are shown in Figure 5. In almost all cases, pre-edge structures in clinopyroxene samples (whether powder, single-crystal or thin-section) were fitted best by three Lorentzian components (e.g., Ito et al., 2025). The positions of fitted Lorentzian components vary between samples, with, for example, the lowest and highest energy components being centred at different energies in samples dominated by Fe^{2+} and Fe^{3+}, respectively. Although we were able to obtain good fits to our spectra, the fitting process was unable to unambiguously identify as many distinct components in pre-edge structures as predicted from theory (Wilke et al., 2001). This is because the pre-edge structures overlap too closely to be distinguished by curve fitting in samples containing both $^{VI}Fe^{2+}$ and $^{VI}Fe^{3+}$.

Centroid energy positions from fitting pre-edge structures in background-corrected Fe-XANES spectra of powdered samples are presented alongside normalised centroid intensities in Figure 6a. The positions of centroids calculated for Olivine and Staurolite are close to the nominal 7112.1 eV average energy for Fe^{2+}-dominated minerals, while the positions of centroids calculated for Fe^{3+}-bearing Sanidine and Aegirine 2 lie slightly above the nominal 7113.5 eV average energy suggested for Fe^{3+}-dominated minerals (Petit et al., 2001; Wilke et al., 2001). Differences in analytical procedure aside, one possible explanation for this is that while crystal particles are likely to be distributed isotropically in our powdered samples, individual particles will not contribute equally to the resulting spectra. Specifically, particles oriented such that they contribute more to the overall signal (such as those in the b-a orientation described by Ito et al. (2025) where X-rays travel down the b-axis and are polarised parallel to the a-axis) will contribute disproportionately more signal from high-eV peaks related to Fe^{3+}, biasing centroids from high-Fe^{3+} samples to correspondingly higher energies. Regardless, all powdered samples except Staurolite, Sanidine and Aegirine 1 lie on a tieline between Olivine and Aegirine 2, suggesting that all of the clinopyroxene samples investigated (with the possible exception of Aegirine 1) are dominated by octahedrally coordinated Fe and, as such, a convex-up yet near-linear relationship between centroid position and $Fe^{3+}/\Sigma Fe$ can be expected (Wilke et al., 2001).

Relationships between centroid positions and clinopyroxene $Fe^{3+}/\Sigma Fe$ contents determined by Mössbauer spectroscopy and EPMA (stoichiometry; Droop, 1987) are presented in Figures 4b and 4c, respectively (Neave et al., 2024a). There is a strong relationship between centroid energy and $Fe^{3+}/\Sigma Fe$ regardless of how $Fe^{3+}/\Sigma Fe$ was deter-

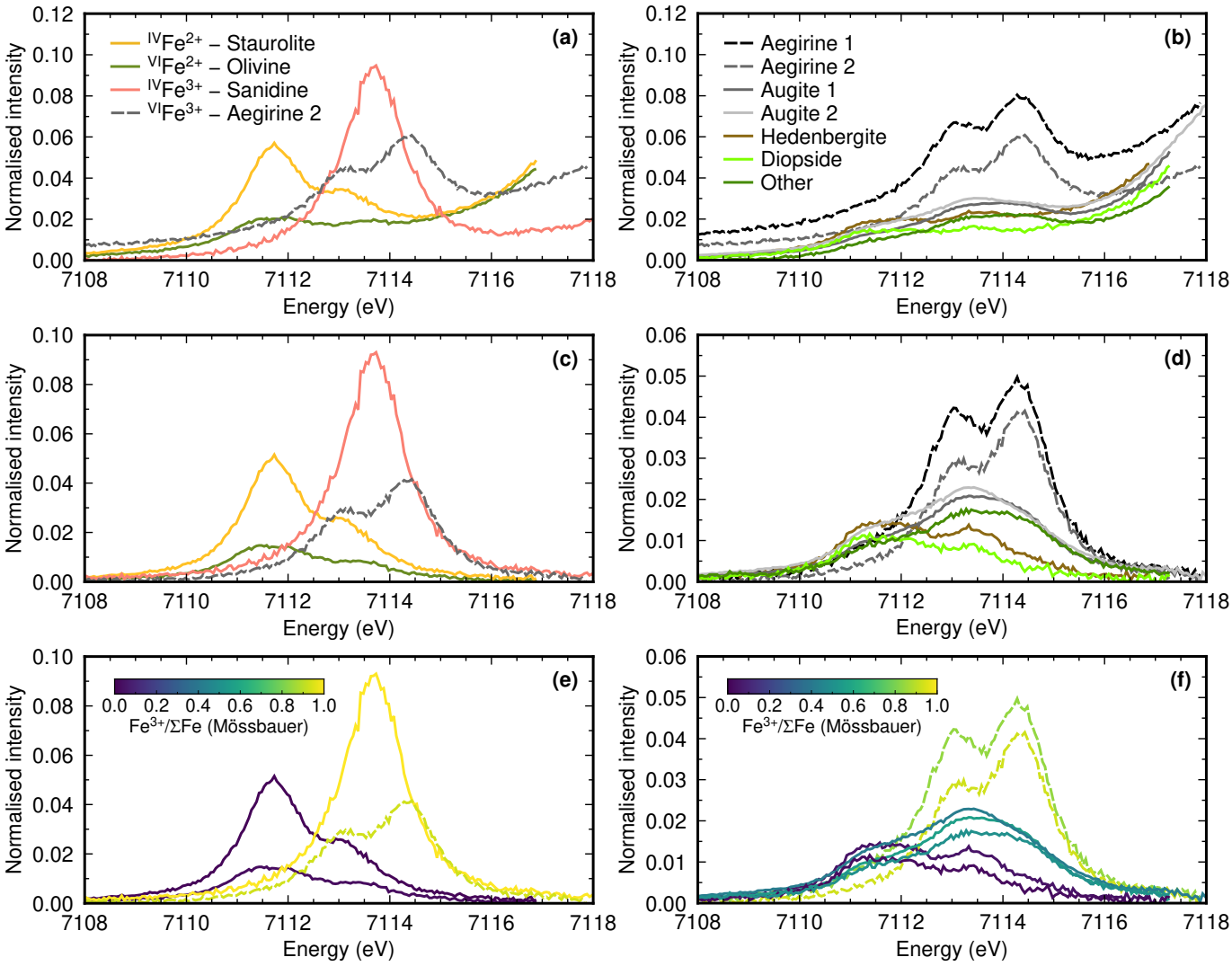

Figure 4. Fe-XANES spectra collected from the Fe K-edge pre-edge region of powdered samples of known Fe valence. (a) Normalised spectra collected from powdered samples of Staurolite, Olivine, Sanidine and Aegirine 2 representing endmembers in Fe valence and coordination relevant to studying Fe valence in clinopyroxene crystals. Spectra were normalised by fitting a linear model to the region 150–280 eV above the E0 position of each spectrum. Compositions are provided in Tables 1 and 3. (b) Normalised spectra collected from powdered clinopyroxene samples for which Fe valence has been determined independently by Mössbauer spectroscopy. Compositions are provided in Tables 1 and 2. Normalisation performed as described for (a). (c and d) Spectra presented in (a) and (c) with backgrounds from the main Fe K-edge subtracted. (e and f) Background-corrected spectra presented in (c) and (d) coloured by Fe valence (i.e., $Fe^{3+}/\Sigma Fe$ contents).

mined (r^2 = 0.97 and 0.96 for Mössbauer spectroscopy and EPMA, respectively). Fitting linear models to our observations suggests that the $Fe^{3+}/\Sigma Fe$ of unknown clinopyroxene powders could potentially be determined with standard errors of estimate (SEEs) of 0.11 or 0.13 based on $Fe^{3+}/\Sigma Fe$ contents from Mössbauer spectroscopy and EPMA, respectively. Fitting polynomial models may more closely reflect the true nature of relationships between centroid position and $Fe^{3+}/\Sigma Fe$ (Figure 4a; Wilke et al., 2001), but uncertainties associated with such models are difficult to evaluate. Moreover, our polynomial models lie mostly within 1 SEE of equivalent linear models and firmly within 2 SEE, and thus do not offer any unambiguous improvement in predictive power over their simpler linear equivalents. Although the energy and intensity resolutions of Fe-XANES spectra we report are much higher than those reported in many previous studies of clinopyroxene (e.g., Dyar et al., 2002; McCanta et al., 2004), it is important to note that we are still unable to predict the $Fe^{3+}/\Sigma Fe$ content of unknown clinopyroxene powders, such as might be obtained through microdrilling (e.g., Davidson and Tepley, 1997), with a precision better than 11 % (1 σ) absolute. This is worse than the ~7 % (1 σ absolute) precision of stoichiometric determinations that can readily be obtained for most magmatic crystals by EPMA (Neave et al., 2024a; Lamb et al., 2024). More reference materials with externally determined $Fe^{3+}/\Sigma Fe$

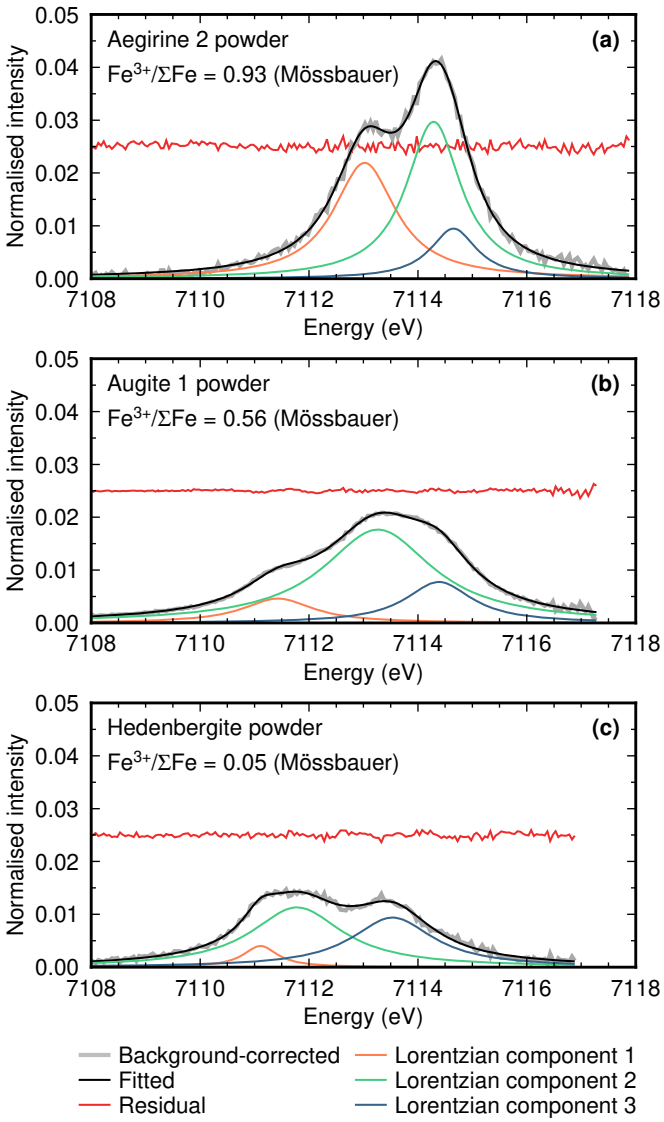

Figure 5. Examples of fits obtained to pre-edge structures in powdered clinopyroxene samples using Larch XAS viewer (Newville, 2013). Samples shown range from Fe^{3+}-rich Aegirine 2, to Fe^{2+}-rich Hedenbergite and Augite 1 that contains nearly equal proportions of Fe^{2+} and Fe^{3+}. Almost all samples were fitted best with three Lorentzian components regardless of the expected number of components from theory (Wilke et al., 2001). Residuals are offset for clarity but are shown at true scale.

contents would be required to improve the precision of high-throughput XANES-based determinations of $Fe^{3+}/\Sigma Fe$ in clinopyroxene powders, and to bring the precision of these determinations into line with the ∼1 % (1 σ absolute) precision that can be routinely achieved when analysing volcanic glasses (Cottrell et al., 2009; Zhang et al., 2018). However, it is unclear whether this would represent a prudent use of beamtime given the performance of considerably more accessible EPMA-based alternatives.

4.2 Oriented clinopyroxene crystals of known Fe valence

Background-corrected Fe-XANES spectra collected from three single-crystal samples across the pre-edge region of the Fe K-edge—Hedenbergite, Augite 1 and Aegirine 2—are shown in Figure 7. These samples were oriented with their a-c planes parallel to the beamline optics and span the full range of $Fe^{3+}/\Sigma Fe$ contents investigated here (0.05–0.93 according to Mössbauer spectroscopy; Neave et al., 2024a). We focussed on the a-c plane because we could access the greatest range of orientations between the a- and c-axes across the largest number of samples. Spectra were collected at a range of angles in the a-c plane, and are reported in terms of angular distances between the incident beam and the a-axis of the crystal in the direction of the c-axis (Figure 1). As such, an angle of 0° means that the incident beam was parallel to the a-axis (with the beam polarised in the a-b plane), and an angle of ∼110° means that the incident beam was parallel to the c-axis. Not all angles were accessible in all samples because of variable sample geometries and our limited ability to orient samples at the beamline.

In line with observations from powdered samples (Figure 4), the intensity of pre-edge structures increases as the $Fe^{3+}/\Sigma Fe$ content of samples increases (Figure 7); the intensity of pre-edge structures is generally higher in single-crystal samples than powdered samples. As documented in previous clinopyroxene Fe-XANES work (Dyar et al., 2002; Steven et al., 2022), the shape of pre-edge structures depends strongly on crystal orientation, with the effect being more prominent in samples with greater $Fe^{3+}/\Sigma Fe$. For example, pre-edge structures in Fe^{3+}-rich Aegirine 2 can be mostly explained by two components centred at ∼7113.0 eV and ∼7114.3 eV (though the latter is generally accounted for by mixing two Lorentzian components; Figure 5a), with the ∼7113.0 eV component being more prominent when the incident beam is close to the c-axis and the ∼7114.3 eV component being more prominent when the incident beam is close to the a-axis (Figure 7a). The position of the pre-edge centroid thus changes significantly as a function of orientation: the centroid is located at ∼7114.0 eV when the incident beam is close to the a-axis and at ∼7113.5 eV when the incident beam is close to the c-axis (Figure 8a), which is well outside typical uncertainties of fitted centroid positions that are on the order of ±0.02 eV (1 σ).

Augite 1, which contains roughly equal proportions of Fe^{2+} and Fe^{3+}, shows similar trends in pre-edge structures to Fe^{3+}-rich Aegirine 2, though a third, lower-energy component associated with Fe^{2+} and centred at ∼7111.4 eV is required to fully described the structure of the pre-edge region in addition to the two components centred at ∼7113.0 eV and ∼7114.3 eV. The ∼7113.0 eV component is more prominent when the incident beam is close to the c-axis and the ∼7114.3 eV component is more prominent when the incident beam is close to the a-axis, resulting in shifts in centroid energy as a function of orientation that are similar in form to those observed for Aegirine 2, albeit less intense (Figure 8b).

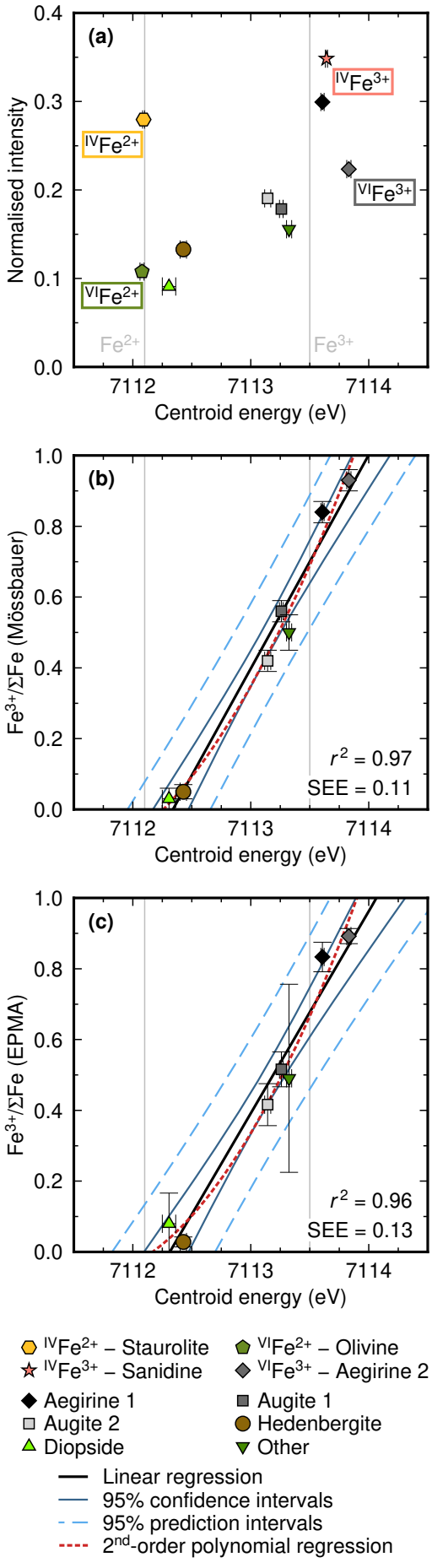

Figure 6. (a) Positions and intensities of centroids fitted to pre-edge structures in background-corrected Fe-XANES spectra of powdered samples. All clinopyroxene samples, with the exception of Aegirine 1, lie between notional $^{VI}Fe^{2+}$ and $^{VI}Fe^{3+}$ endmembers defined by Olivine and Aegirine 2, respectively; error bars are 1 σ uncertainties in fitted centroid positions. Nominal centroid positions for Fe^{2+}- and Fe^{3+}-dominated compounds are shown for reference (e.g., Wilke et al., 2001). (b and c) Relationships between centroid position and $Fe^{3+}/\Sigma Fe$ determined by (b) Mössbauer spectroscopy and (c) electron probe microanalysis (EPMA) reported by Neave et al. (2024a); error bars are 1 σ uncertainties. Although relationships between centroid position and $Fe^{3+}/\Sigma Fe$ are theoretically non-linear (Wilke et al., 2001), and can be fitted as such, polynomial models lie comfortably within the prediction uncertainty of simpler linear models, which are therefore taken forwards.

Pre-edge structures in Fe^{2+}-rich Hedenbergite differ from those in Augite 1 and Aegirine 2. Specifically, three relatively low-intensity components are required to fit Hedenbergite spectra, centred at ~7111.2 eV, ~7111.8 eV and ~7113.6 eV (Figure 5c). Moreover, centroid positions appear to be affected less by clinopyroxene orientation in Hedenbergite than Augite 1 or Aegirine 2 (Figure 8c). This is because low energy components associated with Fe^{2+} have lower absolute intensities than high-energy components associated with Fe^{3+} and thus experience relatively smaller changes in intensity as a function of changing orientation. As such, centroid positions from Fe^{3+}-rich samples like Aegirine 2 that are defined by high-energy components will be more sensitive to changes in orientation than those from Fe^{2+}-rich samples like Hedenbergite that are defined by low-energy components.

Spectra collected from oriented clinopyroxene crystals of known Fe valence reaffirm prior observations that the morphology of pre-edge structures depends strongly on clinopyroxene orientation (e.g., Dyar et al., 2002). Moreover, the nature and magnitude of this dependence itself depends strongly on clinopyroxene $Fe^{3+}/\Sigma Fe$ content (Figure 8d), making it challenging to use Fe-XANES to determine clinopyroxene $Fe^{3+}/\Sigma Fe$ in unknown samples. This challenge can be further illustrated by comparing the positions of centroids determined from powdered samples with those from oriented samples. The centroid fitted to the powdered sample of Aegirine 2 is most similar to centroids fitted to crystal fragments oriented with the incident beam ~20° either side of the a-axis in the a-c plane, or at angles of ~70° and ~90° towards the c-axis from the a-axis. Conversely, the centroid fitted to the powdered sample of Augite 1 is most similar to centroids fitted to crystal fragments oriented with the incident beam ~40° towards the c-axis from the a-axis and approximately down the c-axis itself. Relationships between centroid positions in powdered and oriented samples are less clear for Hedenbergite, though the closest correspondence is found when the incident beam

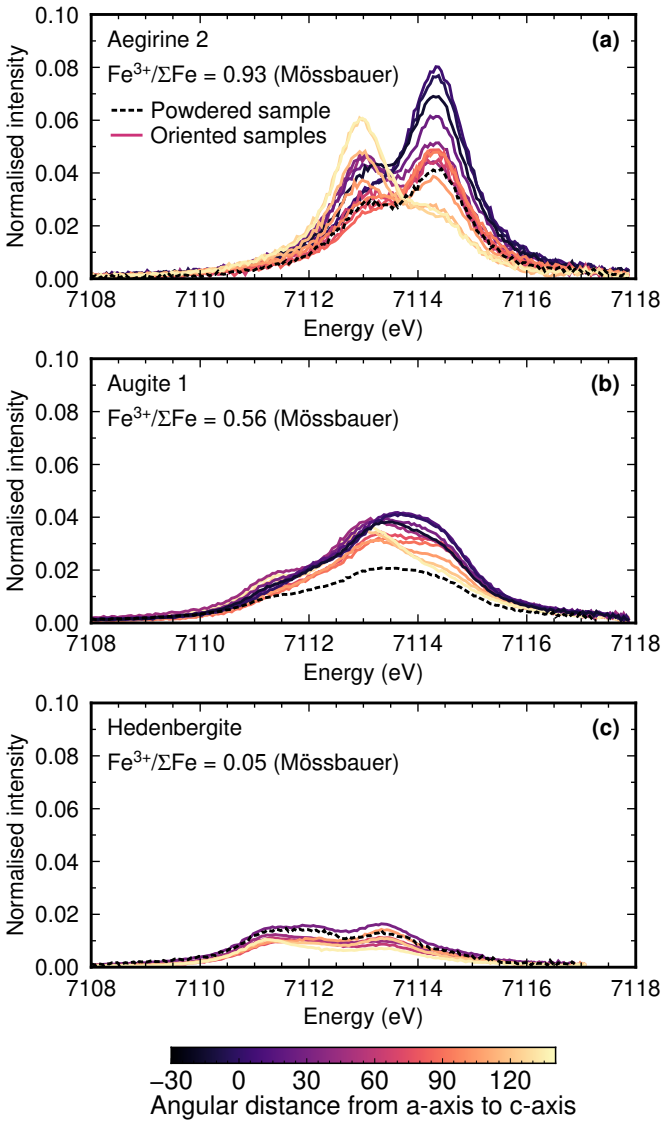

Figure 7. Fe-XANES spectra collected from oriented clinopyroxene samples of known Fe valence across the pre-edge region of the Fe K-edge. Samples were oriented with their a-c planes parallel to beamline optics, and spectra are coloured by the angular distance between the a-axis and the incident beam in the direction of the c-axis (Figure 1). The position and intensity of pre-edge structures change as a function of $Fe^{3+}/\Sigma Fe$, with structures being higher energy and more intense in Aegirine 2 (a) than Hedenbergite (c); structures in Augite 1 (b) are intermediate.

is either at ∼60° towards the c-axis from the a-axis, and when the incident beam was beyond the c-axis, at an angular distance of ∼135° from the a-axis. As such, it is impossible to identify a single angle (a so-called magic angle) at which the centroid positions of oriented samples mimic those of quasi-isotropic powders analogous to that proposed for highly anisotropic phyllosilicate single crystals (Muñoz et al., 2013). Therefore, calibrations to estimate $Fe^{3+}/\Sigma Fe$ in clinopyroxene crystals of unknown Fe valence must either be based on spectra from reference materials collected at known orientations that are also incorporated into regressions for $Fe^{3+}/\Sigma Fe$ or spectra from unknowns and reference materials collected in the same orientations. While the first approach has enabled the $Fe^{3+}/\Sigma Fe$ content of clinopyroxene and amphibole samples to be recovered with uncertainties of ∼6 % (1 σ absolute) when applied across the whole XAS region of the K-edge (e.g., Dyar et al., 2016; Ito et al., 2025), it also requires precisely oriented reference materials to be analysed in numerous orientations. Such approaches can not only be difficult to realise given the challenges associated with securing synchrotron beamtime (simply constructing a calibration curve may take upwards of several hours) but are also contingent on painstaking prior work to document crystal orientations. Here we explore the feasibility of using the second approach—collecting spectra from unknowns and reference materials in similar orientations—to estimate clinopyroxene $Fe^{3+}/\Sigma Fe$ contents from relatively few reference spectra in a routinely deployable way.

4.3 Oriented clinopyroxene crystals of unknown Fe valence

Centroid positions of pre-edge structures in spectra collected from the a-c plane of Augite 3 are shown in Figure 9a. Note that Augite 3 is compositionally distinct from Augite 1 and Augite 2, being both more evolved (lower Mg#, where Mg# = $Mg/(Mg+Fe^{2+})$ on a molar basis) and more enriched in quadrilateral components (Figure 2). While the centroid positions observed for Augite 3 are at lower energies in any given orientation compared with those observed in Augite 1 (Figure 8b), the general sense of centroid position variability as a function of orientation is similar between the two samples. As no Mössbauer spectra were collected from Augite 3, we can use this sample to evaluate our ability to estimate $Fe^{3+}/\Sigma Fe$ in an unknown clinopyroxene by Fe-XANES. Although spectra could be collected close to the c-axis in Hedenbergite, Augite 1 and Aegirine 2, the centroid positions of analyses in the Augite 1 and Aegirine 2 are indistinguishable in these orientations (Figure 8d), meaning that $Fe^{3+}/\Sigma Fe$ can not be derived from pre-edge structures when the incident beam is parallel to the c-axis. We thus collected spectra with the incident beam within 15° of the mid-point between the a- and c-axes (i.e., at 55 ± 15° towards the c-axis from the a-axis in the a-c plane, where ± 15° is a conservative estimate of the precision with which samples could be oriented without a universal stage). Samples of known Fe valence have clearly different centroid positions in these orientations (Figure 8). The resulting linear calibration of $Fe^{3+}/\Sigma Fe$ as a function of centroid energy is shown in Figure 9b; there are insufficient reference materials to justifiably attempt a polynomial calibration. The SEE of the regression based on five spectra constrained by $Fe^{3+}/\Sigma Fe$ determinations from Mössbauer spectroscopy is 0.19, considerably higher than the 0.11 achieved for a fit to wider range of powdered samples (Figure 6b).

Applying the calibration shown in Figure 9b to the two Augite 3 spectra collected within 15° of the midpoint between the a- and c-axes returns $Fe^{3+}/\Sigma Fe$ contents of 0.35 ± 0.19 (1 σ) and 0.40 ± 0.19 (1 σ). Encouragingly,

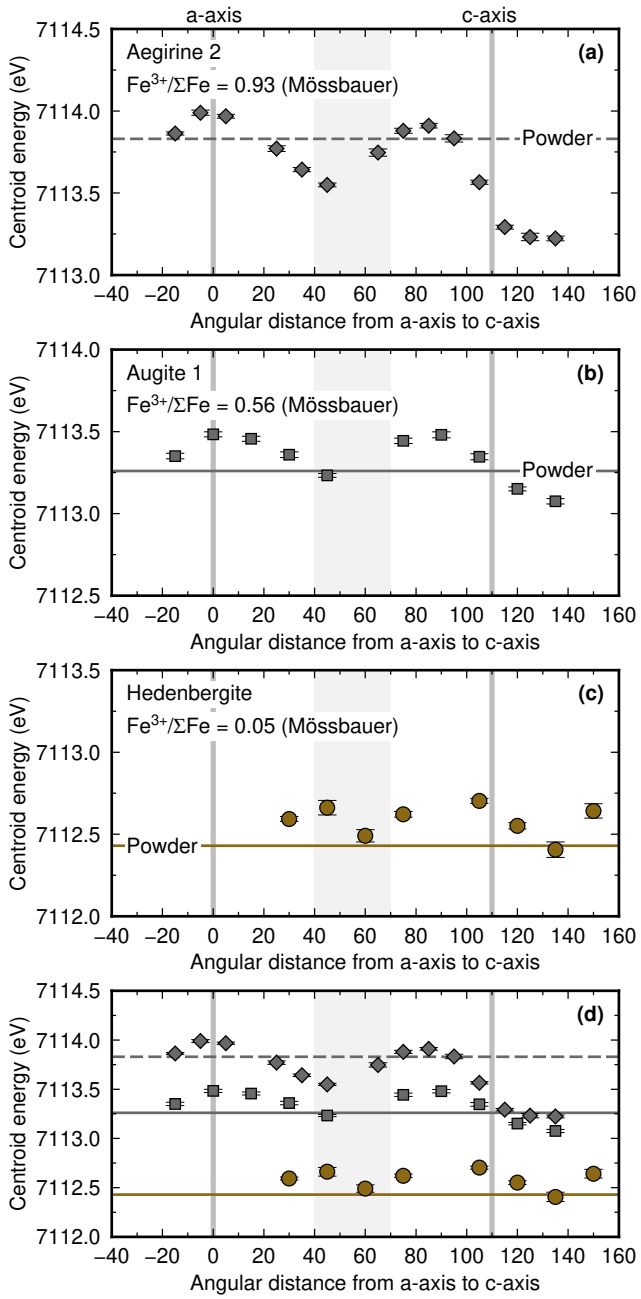

Figure 8. Positions of centroids fitted to pre-edge regions of Fe-XANES spectra collected from clinopyroxene samples of known Fe valence at different orientations. Samples were oriented with their a-c planes parallel to the beamline optics and orientations are reported in terms of the angular distance between the a-axis and the incident beam in the direction of the c-axis (Figure 1); orientations may be associated with uncertainties of up to 15°, though uncertainties in relative differences between angular distances are minimal because the precision of the stage used to rotate mounted samples is high. Centroid positions vary strongly with orientation, and the magnitude of these variations increases with increasing $Fe^{3+}/\Sigma Fe$. Variations in centroid positions comfortably exceed uncertainties in fitted centroid positions. Horizontal lines show centroid positions determined from powdered samples (Figure 6). Centroid positions from powdered samples do not correspond to analyses of oriented samples collected at a fixed angle suggesting that there is no magic angle for powder-equivalent analyses of clinopyroxene crystals (cf., Muñoz et al., 2013). The grey field between the a- and c-axes shows the range of angular distances over which orientation-specific calibrations of $Fe^{3+}/\Sigma Fe$ have been investigated.

these values are comfortably within uncertainty of the value obtained from stoichiometric determinations of $Fe^{3+}/\Sigma Fe$ via EPMA (0.34 ± 0.03 ($1\,\sigma$); Table 2), and are wholly reasonable for magmatic augite (Neave et al., 2024b). This test hence suggests that orientation-specific regressions of centroid position can return estimates of $Fe^{3+}/\Sigma Fe$ that agree with independently obtained values. However, the 19 % ($1\,\sigma$ absolute) uncertainties associated with these estimates are arguably no better than the ~15–20 % ($1\,\sigma$ absolute) previously reported when determining $Fe^{3+}/\Sigma Fe$ from randomly oriented clinopyroxene crystals (Dyar et al., 2002; McCanta et al., 2004). Although crystal orientation effects no doubt contribute to these large uncertainties, the predictive power of the regression is also fundamentally limited by the number of spectra from reference materials.

In order to produce the best possible calibration for use on magmatic crystals, we also calibrated $Fe^{3+}/\Sigma Fe$ as a function of centroid energy for oriented reference materials using $Fe^{3+}/\Sigma Fe$ contents determined by EPMA (Figure 9c). Although $Fe^{3+}/\Sigma Fe$ contents determined stoichiometrically by EPMA are less precise than those from Mössbauer spectroscopy, incorporating Augite 3 into the calibration results in an appreciably lower SEE of 0.12. Moreover, the inclusion of Augite 3 anchors the calibration at compositions expected in many magmatic systems (Figure 3; Neave et al., 2024b).

4.4 Estimating the Fe valence state in magmatic clinopyroxene crystals

Collecting spectra from magmatic crystals in known orientations was challenging without access to a universal stage. We therefore focussed on crystals whose a-c planes were as close to perpendicular to the sample surface as possible, and for which the midpoint between the a- and c-axes was oriented at $45 \pm 15°$ to the sample surface. As such the incident beams for these analyses were oriented at $55 \pm 15°$ from the a-axis in the a-c plane, meaning that we could apply the calibration presented in Figure 9c to estimate $Fe^{3+}/\Sigma Fe$ contents (Figure 10). Centroid positions and estimated $Fe^{3+}/\Sigma Fe$ contents for one crystal from each of Skuggafjöll and Pico are reported in Figure 11. Although we could determine centroid positions with a high level of precision, the modest predictive power of the regression derived from seven reference spectra means that the compositions of magmatic crystals could only be estimated with a precision of 12 % ($1\,\sigma$ absolute).

Mean clinopyroxene $Fe^{3+}/\Sigma Fe$ contents estimated by Fe-XANES for Skuggafjöll and Pico are -0.03 ± 0.06 ($1\,\sigma$; $n = 3$) and 0.21 ± 0.07 ($1\,\sigma$; $n = 3$), respectively. The mean

negative value from Skuggafjöll is a physically meaningless artefact from fitting and should thus be interpreted as being within uncertainty of zero. Although the individual estimates of $Fe^{3+}/\Sigma Fe$ used to calculate these means are associated with considerable uncertainties of 12 % (1 σ absolute), $Fe^{3+}/\Sigma Fe$ contents from Fe-XANES nevertheless overlap with $Fe^{3+}/\Sigma Fe$ contents from EPMA performed on crystals spread across whole thin sections within 2 σ (0.17 ± 0.19 (2 σ; $n = 55$) and 0.29 ± 0.13 (2 σ; $n = 76$), respectively); EPMA was performed on crystals that are texturally equivalent to those on which Fe-XANES was performed. Performing Fe-XANES on magmatic clinopyroxene crystals nevertheless reinforces a key observation from previous EPMA work—clinopyroxene crystals in alkalic samples from Pico have higher mean $Fe^{3+}/\Sigma Fe$ contents than clinopyroxene crystals in tholeiitic samples from Skuggafjöll, with the overlap between these samples reflecting natural variability as well as propagated analytical uncertainty (Neave et al., 2024b). This is important because the pre-edge structures used to estimate $Fe^{3+}/\Sigma Fe$ by Fe-XANES are direct and physically based indicators of the valence state of Fe (Westre et al., 1997), while stoichiometric determinations by EPMA are, by their very nature, indirect (Droop, 1987). Thus, although the determinations of clinopyroxene $Fe^{3+}/\Sigma Fe$ based on Fe-XANES presented here are too imprecise to infer geological processes, they support observations made with other more precise approaches.

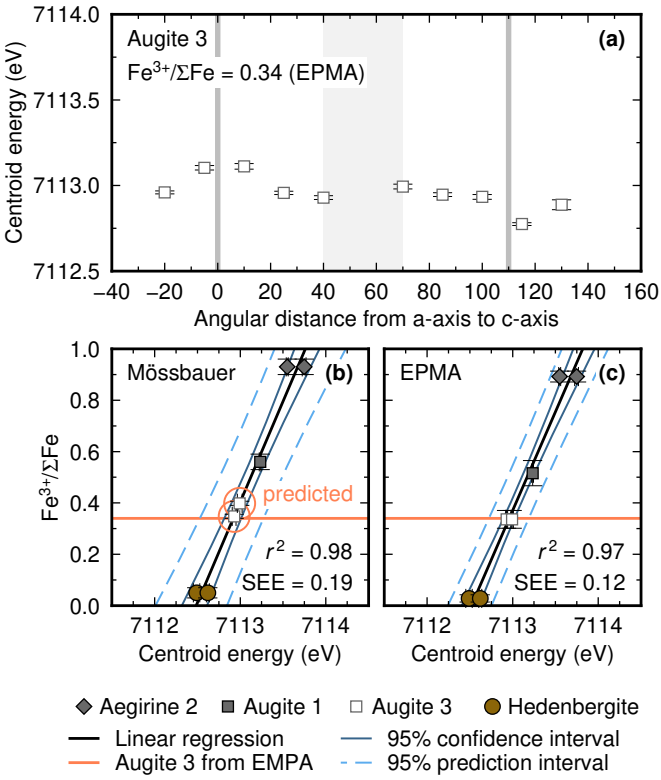

Figure 9. (a) Positions of centroids fitted to pre-edge regions of Fe-XANES spectra collected from an oriented clinopyroxene crystal of unknown Fe valence (Augite 3) at different orientations. Augite 3 was oriented with its a-c plane parallel to the beamline optics. Orientations are reported in terms of the angular distance between the a-axis and the incident beam in the direction of the c-axis and may be associated with uncertainties of up to 15°, though uncertainties in relative differences between angular distances are minimal. (b) Results of predicting the $Fe^{3+}/\Sigma Fe$ content of Augite 3 from centroid positions of spectra collected within 15° of the mid-point between the a- and c-axes using a linear model fitted with five spectra from reference materials measured by Mössbauer spectroscopy in similar orientations. (c) Results of calibrating a linear model for predicting $Fe^{3+}/\Sigma Fe$ from centroid positions using seven spectra from reference materials characterised by EPMA (i.e., stoichiometry). Including Augite 3 improves the precision of the calibration even though clinopyroxene compositions are known less precisely by EPMA than Mössbauer spectroscopy.

5 Conclusions

The increasingly widespread use of synchrotron-based Fe-XANES to determine the valence state of Fe in geological materials over recent decades has considerably advanced our understanding of fO_2 in Earth's interior (Sutton et al., 2020), with analyses of isotropic materials such as glass, spinel and garnet playing particularly important roles (e.g., Berry et al., 2010; Sorbadere et al., 2018; Holycross and Cottrell, 2022). Progress has also been made towards relating structures in pre-edge and XAS regions of the Fe K-edge to the $Fe^{3+}/\Sigma Fe$ content of anisotropic minerals such as clinopyroxene and amphibole (Dyar et al., 2002, 2016; Steven et al., 2022). However, approaches based on using reference materials in known orientations to determine $Fe^{3+}/\Sigma Fe$ in clinopyroxene crystals of unknown orientation are still associated with uncertainties of at least ~8 % (1 σ absolute; Ito et al., 2025). Moreover, such approaches require reference materials to be analysed at a range of precisely known orientations, which is time consuming, dependent on specialist equipment and thus impractical for routinely determining $Fe^{3+}/\Sigma Fe$ in large numbers of crystals. We therefore explored whether clinopyroxene $Fe^{3+}/\Sigma Fe$ could be determined more straightforwardly by analysing powdered samples or unknown samples and reference materials in similar (though not identical) orientations.

Collecting Fe-XANES spectra from powdered clinopyroxene crystals with independently determined $Fe^{3+}/\Sigma Fe$ contents demonstrated that $Fe^{3+}/\Sigma Fe$ can be estimated from small aliquots of powdered crystals that mimic isotropic materials with relative ease. However, our calibration based on centroid positions measured in clinopyroxene powders can only predict $Fe^{3+}/\Sigma Fe$ with a precision of 11 % (1 σ absolute). This modest precision reflects the small calibration dataset of seven reference materials; the $Fe^{3+}/\Sigma Fe$ contents of these reference materials are also associated with non-negligible uncertainties up to 5 % (1 σ absolute). Comparisons with calibrations constructed for determining $Fe^{3+}/\Sigma Fe$ in magmatic glasses with a precision of ~1 % (1 σ absolute) suggests at least three times as many refer-

ence materials would be needed to adequately define the polynomial fits between centroid position and $Fe^{3+}/\Sigma Fe$ expected from theory (Wilke et al., 2001; Zhang et al., 2018).

Spectra collected from single-crystal clinopyroxene samples oriented with their a-c planes parallel to the beamline optics not only affirm prior observations that pre-edge structures and centroid positions depend on crystal orientation (e.g., Dyar et al., 2002), but also highlight that the nature of this dependence varies with clinopyroxene $Fe^{3+}/\Sigma Fe$ content. Given that changes in clinopyroxene composition also correlate with changes in crystal structure, we suggest that many of the correlations between centroid position, orientation and composition ultimately reflect differences in crystal structure between hedenbergite, augite and aegirine. Such differences also affect the wider XAS region (Ito et al., 2025). Therefore, it may be impossible to precisely calibrate $Fe^{3+}/\Sigma Fe$ as a function of centroid position for single-crystal samples across the full range of clinopyroxene $Fe^{3+}/\Sigma Fe$ contents (i.e., $Fe^{3+}/\Sigma Fe$ = 0–1) without incorporating considerable crystallographic information (e.g., Steven et al., 2022).

By focussing on spectra collected from crystals in similar orientations, we demonstrated that the $Fe^{3+}/\Sigma Fe$ content of unknown clinopyroxene crystals can be estimated with a (considerable) 19 % (1 σ absolute) uncertainty by using an orientation-specific calibration grounded with $Fe^{3+}/\Sigma Fe$ determinations from Mössbauer spectroscopy. Using $Fe^{3+}/\Sigma Fe$ determinations from EPMA (i.e., stoichiometry) instead of Mössbauer spectroscopy allowed us to reduce this uncertainty to 12 % (1 σ absolute) for application to magmatic crystals in thin sections from Skuggafjöll in Iceland and Pico in the Azores by expanding the number of reference materials in the calibration dataset. Mean $Fe^{3+}/\Sigma Fe$ contents estimated for a crystal in each of these samples (-0.03 ± 0.12 (2 σ) and 0.24 ± 0.14 (2 σ) for Skuggafjöll and Pico, respectively, with the value for Skuggafjöll being within uncertainty of zero) overlap within uncertainty of compositions determined by EPMA across these thin sections (0.17 ± 0.19 (2 σ) and 0.29 ± 0.13 (2 σ), respectively). Although the precision of our Fe-XANES determinations is insufficient to inform discussions about magma fO_2 conditions or the behaviour of Fe in magmatic clinopyroxene crystals, they do provide physically based evidence that the different clinopyroxene $Fe^{3+}/\Sigma Fe$ contents obtained in these samples by stoichiometry are sound (cf., Neave et al., 2024b). That is, they confirm that magmatic clinopyroxene crystals from the alkalic Pico system in the Azores contain significantly more Fe^{3+} than those from the tholeiitic Skuggafjöll system in Iceland.

Overall, our findings confirm that clinopyroxene Fe-XANES spectra are highly dependent on crystal orientations, and that this dependence is contingent on the complex interplay between clinopyroxene compositions and clinopyroxene mineral structures. Importantly, uncertainties arising from crystal orientation appear to swamp those associated with either the quality of fits to spectral features or the signal-to-noise ratios of the spectra themselves.

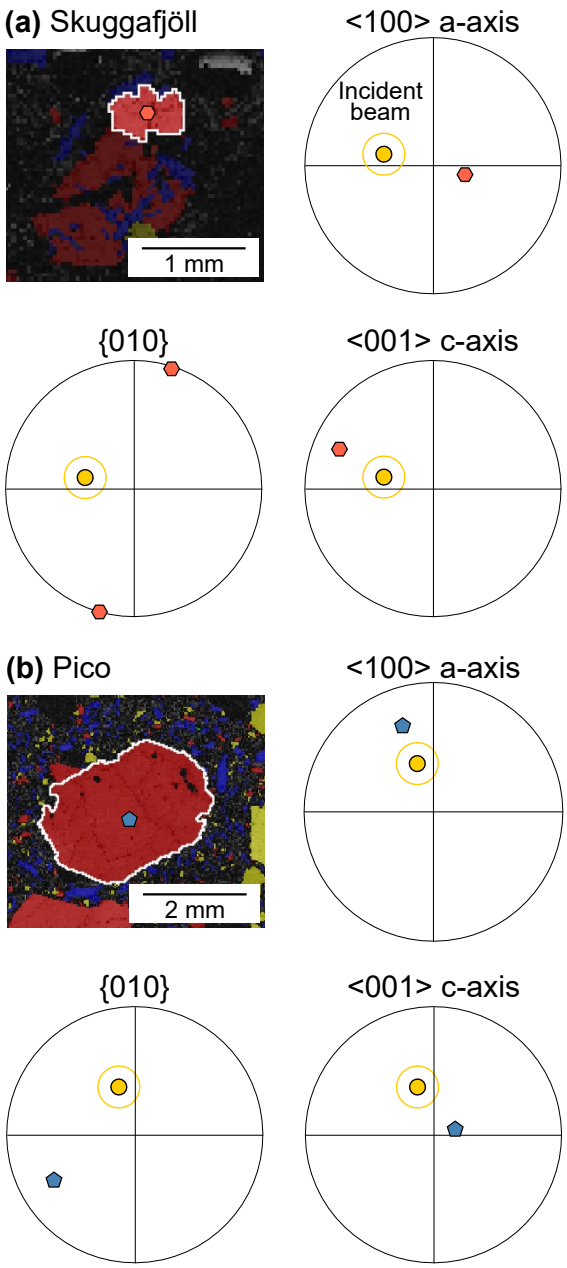

Figure 10. Orientations of individual clinopyroxene crystals analysed in thin sections from each of Skuggafjöll (a) and Pico (b) determined by electron backscatter diffraction (EBSD). Yellow circles show the orientations of incident beams used for Fe-XANES analyses, and other symbols show the orientations of a-, b- and c- axes in the frames of reference shown in coloured phase maps in which red is clinopyroxene, blue is plagioclase and yellow is olivine. Approximate uncertainties in incident beam orientations are shown as yellow circles; uncertainties in crystal orientations are comparable to the size of the points shown. (a) The incident beam is located at ~65° towards the c-axis from the a-axis, and the b-axis is in the plane of the sample. (b) The incident beam is located at ~65° towards the c-axis from the a-axis, though the b-axis is slightly elevated from the sample surface; this was the most favourable orientation present in this thin section.

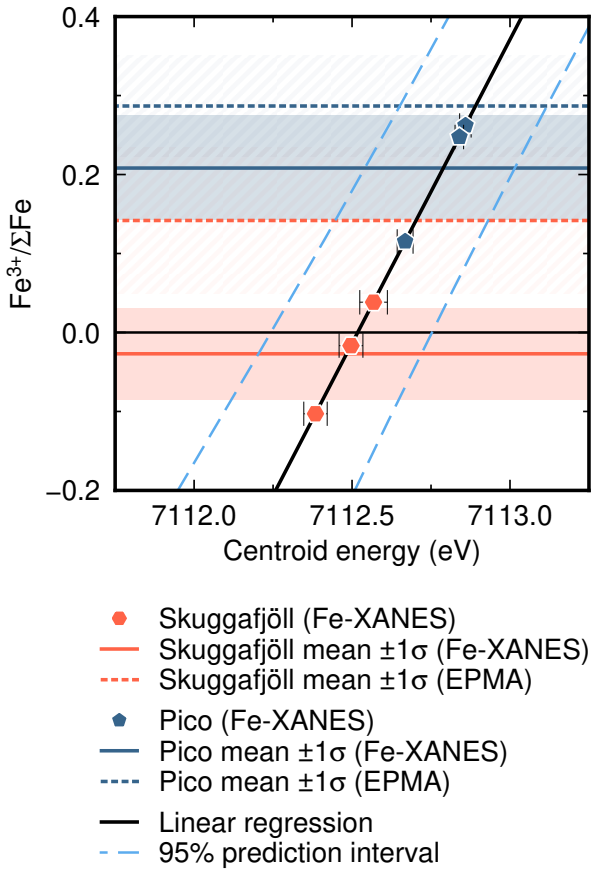

Figure 11. Individual and mean clinopyroxene $Fe^{3+}/\Sigma Fe$ contents estimated by Fe-XANES in samples from Skuggafjöll and Pico compared with mean clinopyroxene $Fe^{3+}/\Sigma Fe$ contents estimated by EPMA (Neave et al., 2024b). Shaded regions show 1 σ intervals associated with means from both approaches. The linear regression used to determine $Fe^{3+}/\Sigma Fe$ contents by Fe-XANES is shown with its associated 95 % prediction intervals (Figure 9c). Although individual clinopyroxene $Fe^{3+}/\Sigma Fe$ contents estimated from Fe-XANES are associated with considerable uncertainties of ∼12 % (1 σ absolute), mean $Fe^{3+}/\Sigma Fe$ contents are within 2 σ with mean $Fe^{3+}/\Sigma Fe$ contents from EPMA (i.e., stoichiometry). Clinopyroxene $Fe^{3+}/\Sigma Fe$ contents Fe-XANES are generally lower than those from EPMA but still reproduce the relatively higher values observed in alkalic samples from Pico than tholeiitic samples from Skuggafjöll (Neave et al., 2024b).

While we can rationalise $Fe^{3+}/\Sigma Fe$ contents obtained from powdered crystals or unknown and reference crystals analysed in similar orientations, the $Fe^{3+}/\Sigma Fe$ contents we obtain from Fe-XANES are much less precise than those obtained from considerably more accessible approaches. The precision of clinopyroxene Fe-XANES could no doubt be improved by characterising a wider array of matrix-matched reference materials in a range of precisely known orientations (e.g., Ito et al., 2025). However, it is unclear if such an endeavour would be worthwhile because much smaller uncertainties of ∼7 % (1 σ absolute) and ∼6 % (1 σ absolute) have already been demonstrated from EPMA-based approaches based on stoichiometry and measuring Lβ/Lα flank ratios that also do not require extensive prior characterisation of clinopyroxene orientations (Neave et al., 2024a; Lamb et al., 2024; Cao et al., 2025). Alongside synchrotron-source Mössbauer spectroscopy (McCammon, 2021), we consider EPMA-based methods to be considerably more practical than synchrotron-based Fe-XANES for determining clinopyroxene $Fe^{3+}/\Sigma Fe$ contents and thereby investigating the nature and causes of fO_2 variability in magmas and their mantle sources.

Acknowledgements

We thank Lewis Hughes for assistance with SEM at the University of Manchester, Ben Buse and Stuart Kearns for assistance with EPMA at the University of Bristol and Konstantin Ignatyev for assistance on Beamline I18 at Diamond Light Source. We thank Catherine McCammon for performing Mössbauer spectroscopy at the Bayerisches Geoinstitut. DAN acknowledges funding from NERC (NE/T011106/1) and the Royal Society (RGS\R1\201344). We also acknowledge Diamond Light Source for time on Beamline I18 under proposal SP31428. All EBSD analyses were carried out in the Scanning Electron Microscopy Shared Research Facility (SEM SRF) at the University of Liverpool. We thank Ery Hughes and two anonymous reviewers for their detailed and constructive reviews and Kate Kiseeva for her editorial handling.

Data, code, and outputs availability

Key data presented in this manuscript are available from the National Geoscience Data Centre hosted by the British Geological Survey in Neave et al. (2026b, https://doi.org/10.5285/c1900414-3e31-4d85-a2b8-3beacdf54392). These data can also be accessed alongside further supporting materials including a table of Fe-XANES centroid positions and fitting parameters in Neave et al. (2026a, https://doi.org/10.48420/29852546.v4). Main text figures and tables are available for download in the online version of this article.

Competing interests

The authors declare no competing interests.

Licence agreement

References

Ballhaus C, Berry RF, Green DH (1991). High pressure experimental calibration of the olivine-orthopyroxene-spinel oxygen geobarometer: implications for the oxidation state of the upper mantle. *Contributions to Mineralogy and Petrology* 107: 27–40. doi:10.1007/BF00311183

Berry AJ, O'Neill HSC, Jayasuriya KD, Campbell SJ, Foran GJ (2003). XANES calibrations for the oxidation state of iron in a silicate glass. *American Mineralogist* 88(7): 967–977. doi:10.2138/am-2003-0704

Berry AJ, Yaxley GM, Woodland AB, Foran GJ (2010). A XANES calibration for determining the oxidation state of iron in mantle garnet. *Chemical Geology* 278(1-2): 31–37. doi:10.1016/j.chemgeo.2010.08.019

Blundy JD, Melekhova E, Ziberna L, Humphreys MCS, Cerantolo V, Brooker RA, McCammon CA, Pichavant M, Ulmer P (2020). Effect of redox on Fe-Mg-Mn exchange between olivine and melt and an oxybarometer for basalts. *Contributions to Mineralogy and Petrology* 7: 103. doi:10.1007/s00410-020-01736-7

Borisov A, Behrens H, Holtz F (2018). Ferric/ferrous ratio in silicate melts: a new model for 1 atm data with special emphasis on the effects of melt composition. *Contributions to Mineralogy and Petrology* 173(12): 98. doi:10.1007/s00410-018-1524-8

Brounce M, Stolper E, Eiler J (2017). Redox variations in Mauna Kea lavas, the oxygen fugacity of the Hawaiian plume, and the role of volcanic gases in Earth's oxygenation. *Proceedings of the National Academy of Sciences* 114(34): 8997–9002. doi:10.1073/pnas.1619527114

Brounce M, Stolper E, Eiler J (2022). The mantle source of basalts from Reunion Island is not more oxidized than the MORB source mantle. *Contributions to Mineralogy and Petrology* 177(1): 7. doi:10.1007/s00410-021-01870-w

Cao Y, Xing CM, Wang CY, Ping X (2025). Determination of the oxidation state of iron in calcic pyroxene using the electron microprobe flank method. *American Mineralogist* doi:10.2138/am-2024-9467

Carmichael ISE (1991). The redox states of basic and silicic magmas: a reflection of their source regions? *Contributions to Mineralogy and Petrology* 106(2): 129–141. doi:10.1007/BF00306429

Cottrell E, Birner SK, Brounce M, Davis FA, Waters LE, Kelley KA (2022). Oxygen Fugacity Across Tectonic Settings. In Moretti R, Neuville D (eds.) *Magma Redox Geochimistry, Geophysical Monograph 266*, pp. 33–61. John Wiley & Sons, Inc. doi:10.1002/9781119473206.ch3

Cottrell E, Kelley K, Lanzirotti A, Fischer RA (2009). High-precision determination of iron oxidation state in silicate glasses using XANES. *Chemical Geology* 268(3-4): 167–179. doi:10.1016/j.chemgeo.2009.08.008

Cottrell E, Kelley KA (2011). The oxidation state of Fe in MORB glasses and the oxygen fugacity of the upper mantle. *Earth and Planetary Science Letters* 305(3-4): 270–282. doi:10.1016/j.epsl.2011.03.014

Cottrell E, Lanzirotti A, Mysen B, Birner S, Kelley K, Botcharnikov RE, Davis F, Newville M (2018). A Mössbauer-based XANES calibration for hydrous basalt glasses reveals radiation-induced oxidation of Fe. *American Mineralogist* 103: 489–501. doi:10.2138/am-2018-6268

Davidson JP, Tepley FJ (1997). Recharge in volcanic systems: Evidence from isotope profiles of phenocrysts. *Science* 275(5301): 826–829. doi:10.1126/science.275.5301.826

Droop GTR (1987). A general equation for Estimating Fe^{3+} concentrations in ferromagnesian silicates and oxides from microprobe analyses, using stoichiometric criteria. *Mineralogical Magazine* 51(361): 431–435. doi:10.1180/minmag.1987.051.361.10

Dyar MD, Breves EA, Gunter ME, Lanzirotti A, Tucker JM, Carey CJ, Peel SE, Brown EB, Oberti R, Lerotic M, Delaney JS (2016). Use of multivariate analysis for synchrotron micro-XANES analysis of iron valence state in amphiboles. *American Mineralogist* 101(5): 1171–1189. doi:10.2138/am-2016-5556

Dyar MD, Gunter ME, Delany JS, Lanzarotti AA, Sutton SR (2002). Systematics in the structure and XANES spectra of pyroxenes, amphiboles, and micas as derived from oriented single crystals. *Canadian Mineralogist* 40(5): 1375–1393. doi:10.2113/gscanmin.40.5.1375

Frost BR (1991). Introduction to oxygen fugacity and its petrologic importance. *Reviews in Mineralogy and Geochemistry* 25: 1–9. doi:10.1515/9781501508684-004

van Gerve TD, Neave DA, Wieser P, Lamadrid H, Hulsbosch N, Namur O (2024). The origin and differentiation of CO_2-rich primary melts in Ocean Island volcanoes: Integrating 3D X-ray tomography with chemical microanalysis of olivine-hosted melt inclusions from Pico (Azores). *Journal of Petrology* 65: 1–24. doi:10.1093/petrology/egae006

Ghiorso MS, Evans BW (2008). Thermodynamics of rhombohedral oxide solid solutions and a revision of the Fe-Ti two-oxide geothermometer and oxygen-barometer. *American Journal of Science* 308(9): 957–1039. doi:10.2475/09.2008.01

Ghiorso MS, Sack O (1991). Fe-Ti oxide geothermometry: thermodynamic formulation and the estimation of intensive variables in silicic magmas. *Contributions to Mineralogy and Petrology* 108(4): 485–510. doi:10.1007/BF00303452

Hartley ME, Shorttle O, Maclennan J, Moussallam Y, Edmonds M (2017). Olivine-hosted melt inclusions as an archive of redox heterogeneity in magmatic systems. *Earth and Planetary Science Letters* 479: 192–205. doi:10.1016/j.epsl.2017.09.029

Helz RT, Cottrell E, Brounce MN, Kelley KA (2017). Olivine-Melt Relationships and Syneruptive Redox Variations in the 1959 Eruption of Kīlauea Volcano as Revealed by XANES. *Journal of Volcanology and Geothermal Research* 333-334: 1–14. doi:10.1016/j.jvolgeores.2016.12.006

Holycross M, Cottrell E (2022). Experimental quantification of vanadium partitioning between eclogitic minerals (garnet, clinopyroxene, rutile) and silicate melt as a function of temperature and oxygen fugacity. *Contributions to Mineralogy and Petrology* 177(2): 1–23. doi:10.1007/s00410-022-01888-8

Ito T, Wallis SR, Takahashi Y (2025). Accurate XANES determination of microscale Fe redox state in clinopyroxene: a multivariate approach with polarization-dependent Fe K-edge XAFS. *American Mineralogist* doi:10.2138/am-2024-9712

Kelley KA, Cottrell E (2009). Water and the Oxidation State of Subduction Zone Magmas. *Science* 325(5940): 605–607. doi:10.1126/science.1174156

Kress VC, Carmichael ISE (1991). The compressibility of silicate liquids containing Fe_2O_3 and the effect of composition, temperature, oxygen fugacity and pressure on their redox states. *Contributions to Mineralogy and Petrology* 108(1-2): 82–92. doi:10.1007/BF00307328

Lamb W, Mott A, Popp R, Chmiel G (2024). Estimating values of $Fe^{3+}/\Sigma Fe$ in pyroxenes with the electron microprobe. *Lithos* 484-485: 107746. doi:10.1016/j.lithos.2024.107746

McCammon C (2021). Mössbauer Spectroscopy with High Spatial Resolution: Spotlight on Geoscience. In Yoshida Y, Langouche G (eds.) *Modern Mössbauer Spectroscopy*, vol. 137, pp. 221–266. Springer Singapore, Singapore. doi:10.1007/978-981-15-9422-9_5

McCanta MC, Dyar MD, Rutherford MJ, Delaney JS (2004). Iron partitioning between basaltic melts and clinopyroxene as a function of oxygen fugacity. *American Mineralogist* 89(11-12): 1685–1693. doi:10.2138/am-2004-11-1214

Morimoto N, Fabries J, Ferguson AK, Ginzburg IV, Ross M, Seifert FA, Zussman J, Aoki K, Gottardi G (1988). Nomenclature of pyroxenes. *American Mineralogist* 73: 1123–1133. doi:10.1007/BF01226262

Moussallam Y, Edmonds M, Scaillet B, Peters N, Gennaro E, Sides I, Oppenheimer C (2016). The impact of degassing on the oxidation state of basaltic magmas: A case study of Kīlauea volcano. *Earth and Planetary Science Letters* 450: 317–325. doi:10.1016/j.epsl.2016.06.031

Moussallam Y, Longpré MA, McCammon CA, Gómez-Ulla A, Rose-Koga EF, Scaillet B, Peters N, Gennaro E, Paris R, Oppenheimer C (2019). Mantle plumes are oxidised. *Earth and Planetary Science Letters* 527: 115798. doi:10.1016/j.epsl.2019.115798

Moussallam Y, Oppenheimer C, Scaillet B, Gaillard F, Kyle P, Peters N, Hartley ME, Berlo K, Donovan A (2014). Tracking the changing oxidation state of Erebus magmas, from mantle to surface, driven by magma ascent and degassing. *Earth and Planetary Science Letters* 393: 200–209. doi:10.1016/j.epsl.2014.02.055

Muñoz M, Vidal O, Marcaillou C, Pascarelli S, Mathon O, Farges F (2013). Iron oxidation state in phyllosilicate single crystals using Fe- K pre-edge and XANES spectroscopy: Effects of the linear polarization of the synchrotron X-ray beam. *American Mineralogist* 98: 1187–1197. doi:10.2138/am.2013.4289

Neave D, Mariani E, Hartley M, Stewart A, Shorttle O, Humphreys M (2026a). Fe-X-ray Absorption Near Edge Spectroscopy (Fe-XANES) spectra from clinopyroxene powders and crystals with known and unknown Fe3+/FeTotal contents with supporting major element compositions from EPMA, Fe3+/FeTotal contents from Mossbauer spectroscopy and crystal orientation data from EBSD. University of Manchester. doi:10.48420/29852546.v4

Neave DA, Maclennan J, Hartley ME, Edmonds M, Thordarson T (2014). Crystal storage and transfer in basaltic systems: the Skuggafjöll eruption, Iceland. *Journal of Petrology* 55(12): 2311–2346. doi:10.1093/petrology/egu058

Neave DA, Mariani E, Stewart AG, Hartley ME, Shorttle O, Humphreys MCS (2026b). Fe-X-ray Absorption Near Edge Spectroscopy (Fe-XANES) spectra from clinopyroxene powders and crystals with known and unknown Fe3+/FeTotal contents with supporting major element compositions from EPMA and crystal orientation data from EBSD. NERC EDS National Geoscience Data Centre. doi:10.5285/c1900414-3e31-4d85-a2b8-3beacdf54392

Neave DA, Stewart AG, Hartley ME, McCammon C (2024a). Re-evaluating stoichiometric estimates of iron valence in magmatic clinopyroxene crystals. *Contributions to Mineralogy and Petrology* 179(5): 17. doi:10.1007/s00410-023-02080-2

Neave DA, Stewart AG, Hartley ME, Namur O (2024b). Iron valence systematics in clinopyroxene crystals from ocean island basalts. *Contributions to Mineralogy and Petrology* 179(6): 67. doi:10.1007/s00410-024-02144-x

Newville M (2013). Larch: An Analysis Package for XAFS and Related Spectroscopies. *Journal of Physics: Conference Series* 430: 012007. doi:10.1088/1742-6596/430/1/012007

Nicklas RW, Hahn RK, Willhite LN, Jackson MG, Zanon V, Arevalo R, Day JM (2022). Oxidized mantle sources of HIMU- and EM-type Ocean Island Basalts. *Chemical Geology* 602: 120901. doi:10.1016/j.chemgeo.2022.120901

Nikolaev GS, Ariskin AA, Barmina GS, Nazarov MA, Almeev RR (2016). Test of the Ballhaus–Berry–Green Ol–Opx–Sp oxybarometer and calibration of a new equation for estimating the redox state of melts saturated with olivine and spinel. *Geochemistry International* 54(4): 301–320. doi:10.1134/S0016702916040078

O'Neill HSC (1987). Quartz-fayalite-iron and quartz-fayalite-magnetite equilibria and the free energy of formation of fayalite (Fe_2SiO_4) and magnetite (Fe_3O_4). *American Mineralogist* 72(1-2): 67–75

O'Neill HSC, Berry AJ, Mallmann G (2018). The oxidation state of iron in Mid-Ocean Ridge Basaltic (MORB) glasses: Implications for their petrogenesis and oxygen fugacities. *Earth and Planetary Science Letters* 504: 152–162. doi:10.1016/j.epsl.2018.10.002

Petit PE, Farges F, Wilke M, Solé VA (2001). Determination of the iron oxidation state in Earth materials using XANES pre-edge information. *Journal of Synchrotron Radiation* 8(2): 952–954. doi:10.1107/S0909049500021063

Prescher C, McCammon C, Dubrovinsky L (2012). *MossA*: a program for analyzing energy-domain Mössbauer spectra from conventional and synchrotron sources. *Journal of Applied Crystallography* 45(2): 329–331. doi:10.1107/S0021889812004979

Prior DJ, Boyle AP, Brenker FE, Cheadle MC, Austin D, Lopez G, Peruzzo L, Potts GJ, Reddy S, Spiess R, Timms NE, Trimby P, Wheeler J, Zetterström L (1999). The application of electron backscatter diffraction and orientation contrast imaging in the SEM to textural problems in rocks. *American Mineralogist* 84(11-12): 1741–1759. doi:10.2138/am-1999-11-1204

Prior DJ, Mariani E, Wheeler J (2009). EBSD in the earth sciences: applications, common practice, and challenges. In Schwartz AJ, Kumar M, Adams BL, Field DP (eds.) *Electron backscatter diffraction in materials science*, pp. 345–360. Springer. doi:10.1007/978-0-387-88136-2_26

Reay A, Johnstone R, Kawachi Y (1989). Kaersutite, a possible international microprobe standard. *Geostandards and Geoanalytical Research* 13(1): 187–190. doi:10.1111/j.1751-908X.1989.tb00471.x

Shorttle O, Moussallam Y, Hartley ME, Maclennan J, Edmonds M, Murton BJ (2015). Fe-XANES analyses of Reykjanes Ridge basalts: Implications for oceanic crust's role in the solid Earth oxygen cycle. *Earth and Planetary Science Letters* 427: 272–285. doi:10.1016/j.epsl.2015.07.017

Sorbadere F, Laurenz V, Frost D, Wenz M, Rosenthal A, McCammon C, Rivard C (2018). The behaviour of ferric iron during partial melting of peridotite. *Geochimica et Cosmochimica Acta* 239: 235–254. doi:10.1016/j.gca.2018.07.019

Steven CJ, Dyar MD, McCanta M, Newville M, Lanzirotti A (2022). The absorption indicatrix as an empirical model to describe anisotropy in X-ray absorption spectra of pyroxenes. *American Mineralogist* 107(4): 654–663. doi:10.2138/am-2021-7950

Sutton SR, Lanzirotti A, Newville M, Dyar MD, Delaney J (2020). Oxybarometry and valence quantification based on microscale X-ray absorption fine structure (XAFS) spectroscopy of multivalent elements. *Chemical Geology* 531(May 2019): 119305. doi:10.1016/j.chemgeo.2019.119305

Taracsák Z, Longpré MA, Tartèse R, Burgess R, Edmonds M, Hartley ME (2022). Highly oxidising conditions in volatile-rich El Hierro magmas: implications for ocean island magmatism. *Journal of Petrology* 63: 1–21. doi:10.1093/petrology/egac011

Westre TE, Kennepohl P, DeWitt JG, Hedman B, Hodgson KO, Solomon EI (1997). A multiplet analysis of Fe K-edge 1s → 3d pre-Edge features of iron complexes. *Journal of the American Chemical Society* 119(27): 6297–6314. doi:10.1021/ja964352a

Wilke M, Farges F, Partzsch GM, Schmidt C, Behrens H (2007). Speciation of Fe in silicate glasses and melts by in-situ XANES spectroscopy. *American Mineralogist* 92(1): 44–56. doi:10.2138/am.2007.1976

Wilke M, Farges F, Petit PE, Brown GE, Martin F (2001). Oxidation state and coordination of Fe in minerals: An FeK- XANES spectroscopic study. *American Mineralogist* 86(5-6): 714–730. doi:10.2138/am-2001-5-612

Wood BJ, Bryndzia LT, Johnson KE (1990). Mantle oxidation state and its relationship to tectonic environment and fluid speciation. *Science* 248(4953): 337. doi:10.1126/science.248.4953.3

Zhang HL, Cottrell E, Solheid PA, Kelley KA, Hirschmann MM (2018). Determination of $Fe^{3+}/\Sigma Fe$ of XANES basaltic glass standards by Mössbauer spectroscopy and its application to the oxidation state of iron in MORB. *Chemical Geology* 479: 166–175. doi:10.1016/j.chemgeo.2018.01.006